Spring 2021

Powering IoT Sensors with RF Energy Harvesting

Austin Rothschild

Kristi Nguyen

SANTA CLARA UNIVERSITY

Department of Electrical & Computer Engineering

I HEREBY RECOMMEND THAT THE THESIS PREPARED
UNDER MY SUPERVISION BY

Austin Rothschild & Kristi Nguyen

ENTITLED

Powering IoT Sensors with RF Energy Harvesting

BE ACCEPTED IN PARTIAL FULFILLMENT OF THE REQUIREMENTS
FOR THE DEGREE OF

BACHELOR OF SCIENCE
IN
ELECTRICAL ENGINEERING

June 4 2021

Thesis Advisor(s) date

Shoba Krishnan 6/9/2021

Department Chair(s) (use separate line for each chair) date

Powering IoT Sensors with RF Energy Harvesting

By

Austin Rothschild & Kristi Nguyen

SENIOR DESIGN PROJECT REPORT

Submitted to
the Department of Electrical & Computer Engineering

of

SANTA CLARA UNIVERSITY

in Partial Fulfillment of the Requirements
for the degree of
Bachelor of Science in Electrical Engineering

Santa Clara, California

Spring 2021

Contents

List of Figures

List of Tables

Acknowledgements

We are very grateful for the support we have received from multiple parties over the course of this project's duration. Firstly, we'd like to acknowledge Dr. Kurt Schab for his continued academic support on this project. His advising helped us turn our initial ideas into reality. Additionally, we'd like to thank Dr. Shoba Krishnan and Yohannes Kahsai for lending us lab equipment to carry out our project experiments. Without your help, we would have little to show for our efforts. Lastly, we appreciate Texas Instruments for sending us free evaluation boards in order to physically validate our final design.

Abstract

There is a need to power Internet of Things (IoT) applications that require frequent, expensive, and/or dangerous battery replacements. Radio-frequency energy harvesting (RFEH) is a possible alternative source of power for select IoT sensor applications. In comparison to other methods of energy harvesting, RFEH has the smallest incident power densities and therefore comes with many design challenges.

In this project we implement a novel RFEH system powered via a dedicated transmitter. A planar inverted-F antenna (PIFA) and voltage doubler circuit form the designed rectenna (rectifier + antenna) and the system is implemented on a custom PCB to carry out RF-to-DC conversion. The system's feasibility is demonstrated by powering a commercial power management unit (PMU) and temperature sensor over a test duration of eight hours.

1 Background and Motivation

1.1 History

The idea of wireless power transfer (WPT) has existed since the rise of modern electrical engineering in the late 19th century. Nikola Tesla was the first to conceive of the usefulness of WPT, declaring the ability to transfer energy without physical connections or wiring as, "an all-surpassing importance to man" [2]. However, a limitation of WPT systems are low-input powers, not only making system design difficult, but also restricting its application to specific types of loads.

Fortunately, WPT and radio-frequency energy harvesting (RFEH) are now seen as promising future technology due to recent advances in CMOS technology and the ability to utilize low-input powers in small form-factor devices. The exponential increase in electrical computing efficiency is known as *Koomey's Law*, which states that the number of computations per Joule of energy dissipated doubles about every 1.57 years [3]. This trend is visualized in Fig. 1 over the time period of 1940 to 2010.

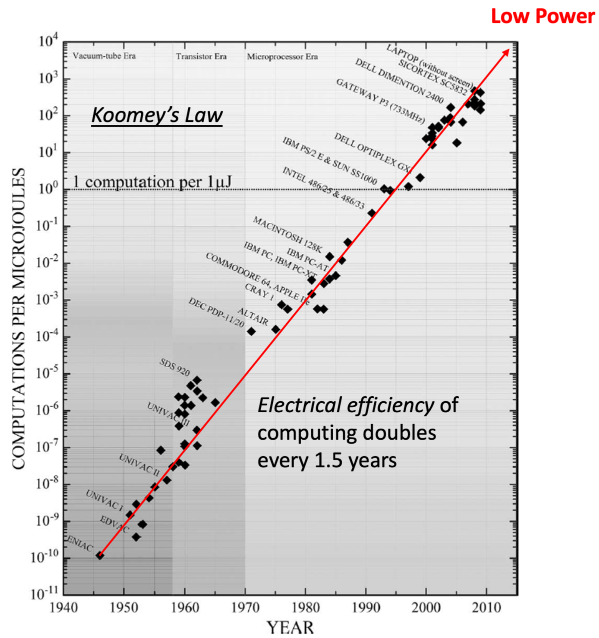

Figure 1: Number of computations per micro-Joules averaged over an hour. A micro-Joule is the sum of 1-μW power during 1s, or 100 nW during 10s [3].

The trend of increasing computational efficiency indicates a future where many devices will operate with minimal power consumption. As a result, RFEH systems will be able to act as practical power sources for a select class of devices. A potential target application of RFEH are Internet of Things (IoT) devices. In the coming years, IoT low-power sensors are expected to be an ubiquitous technology, and RFEH provides a potentially low-cost and enduring alternative to batteries.

Comprised of large sensor networks connected via communication channels, IoT grids require complex wiring schemes or dedicated batteries at the device level [1]. As the world becomes more and more connected, the efficient manufacturing and maintenance of IoT devices will become an urgent matter; by 2030, the number of connected devices is predicted to reach 125 billion [4]. Powering these sensor networks via wired power-grid or primary batteries will soon become infeasible due to cabling costs and the finite lifespan of batteries, which require maintenance and replacement. As an alternative solution, energy supplied by dedicated RF sources will allow IoT networks to be powered wirelessly.

1.2 Technical/Theoretical Background

In far-field WPT systems, an antenna and rectifier, abbreviated as "rectenna," carries out the process of converting RF input to usable direct current (DC) output. First developed by William C. Brown in the 1960's [5], rectennas are devices that can supply energy to traditional low-input power applications and theoretically support infinite device lifetime by removing the need for dedicated batteries with a finite energy supply.

The challenge of designing an efficient WPT system is sustaining a high RF-to-DC conversion efficiency, as the system's efficiency is a function of input power levels, operation frequency, and discrete component properties. These factors change the input impedance of the rectifier network, causing the receive antenna to be mismatched with the rectifier, thus leading to loss of input power and lower conversion efficiency. Therefore, a realized system must be designed with the operating conditions known prior to the physical design. A simplified block diagram of an RFEH system is shown in Fig. 3. Such a system has many components that introduce loss and lower the conversion efficiency from its maximum value of 100%. Because the input-power levels of the system are already low, significant effort needs to be made to ensure proper impedance matching between components.

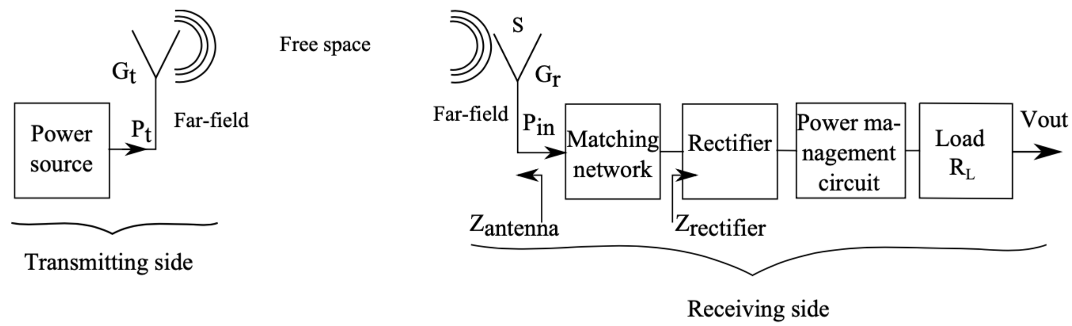

Figure 2: Block diagram of a far-field WPT system [6]. A matching network is utilized to ensure maximum power transfer at the specified operating conditions.

Many of these IoT sensors operate in conditions where it is infeasible, expensive, or dangerous to replace a battery or to deliver wired power. Examples include health monitoring sensors [7, 8], structural support sensors [9], aircraft structural monitoring sensors [10], and sensors utilized in hazardous environments. Overall, the requirements for such sensors include:

1. Small size
2. Low maintenance
3. Unknown exact location

This project aims to meet these system requirements in a manner that maximizes system efficiency by carefully designing each component of a WPT network.

1.3 Functional Block Diagram

A detailed block diagram of the implemented RFEH system is depicted in Fig. 3. The performance parameters which affect system operation are highlighted along with each component. A successful RFEH system attempts to optimize all of these factors simultaneously in order to keep the DC output voltage at a level required by the load application.

The system primarily consists of two elements: the transmitter and receiver. The transmitter has an associated transmit power and carrier frequency, and can either function as an ambient or dedicated source. An ambient source is one that exists for some other purpose, such as mobile broadcast stations or routers used for wireless communications. These sources may have an associated signal modulation scheme which can impact performance. In contrast, a dedicated source is specifically designed to supply power to a select receiver/load side, resulting in higher efficiencies. The transmit antenna can be optimized depending on the target application. For example, a high gain antenna is preferred in situations where the rectenna's location is known, allowing for the transmit antenna to supply power over a greater distance compared to an omnidirectional antenna.

Between the transmitter and receiver is a free-space region. An energy harvesting system that captures energy sent over a free-space region greater than the far-field distance $R > 2D^2/\lambda$ (where D is the largest linear dimension of the transmit or receive antenna and λ is the operating wavelength) is classified as a *far-field* RF energy harvester. The received power levels for a far-field energy harvesting system can be accurately modeled by the Friis transmission equation [11]

$$P_{\mathrm{rx}} = P_t \left(1 - |\Gamma_t|^2\right)\left(1 - |\Gamma_r|^2\right)\left(\frac{\lambda}{4\pi R}\right)^2 G_t\left(\theta_t, \phi_t\right) G_r\left(\theta_r, \phi_r\right) \left|\hat{\rho}_t \cdot \hat{\rho}_r\right|^2, \tag{1}$$

where the received power P_{rx} is a function of the power transmitted (P_t), the matching level of the transmitter and receiver (Γ_t &, Γ_r), the operating wavelength (λ), the transmitter-to-receiver separation distance (R), the gain of the transmit and receive antennas (G_t, G_r), and polarization mismatch between the transmit and receive antennas ($|\hat{\rho}_t \cdot \hat{\rho}_r|^2$).

On the receive side, the first element is the antenna. The antenna is designed to be low-gain such that it can receive input RF energy from any direction. The antenna operates over a specified bandwidth to capture the incident carrier signal. Additionally, the antenna must be matched to a nominal system impedance to minimize reflection losses and ensure maximum power transfer. In this case, a nominal system impedance of $Z_0 = 50\ \Omega$ is used.

Likewise, the rectifier needs to be matched to the system impedance. However, challenges arise as the rectifier's input impedance non-linearly varies as a function of frequency, input power, and load impedance. Thus, a robust simulation model that can capture and represent these effects is crucial for the design of the system.

The output of the rectifier is interfaced with a power management unit (PMU) to store energy and drive the load application. Ideally, the PMU operates in a region that presents a fixed DC resistance to the rectifier, allowing the rectifier to be optimally matched to this value. The load application has its own specifications, such as power consumption and usage period, in addition to minimum driving conditions required for the system to initially be powered.

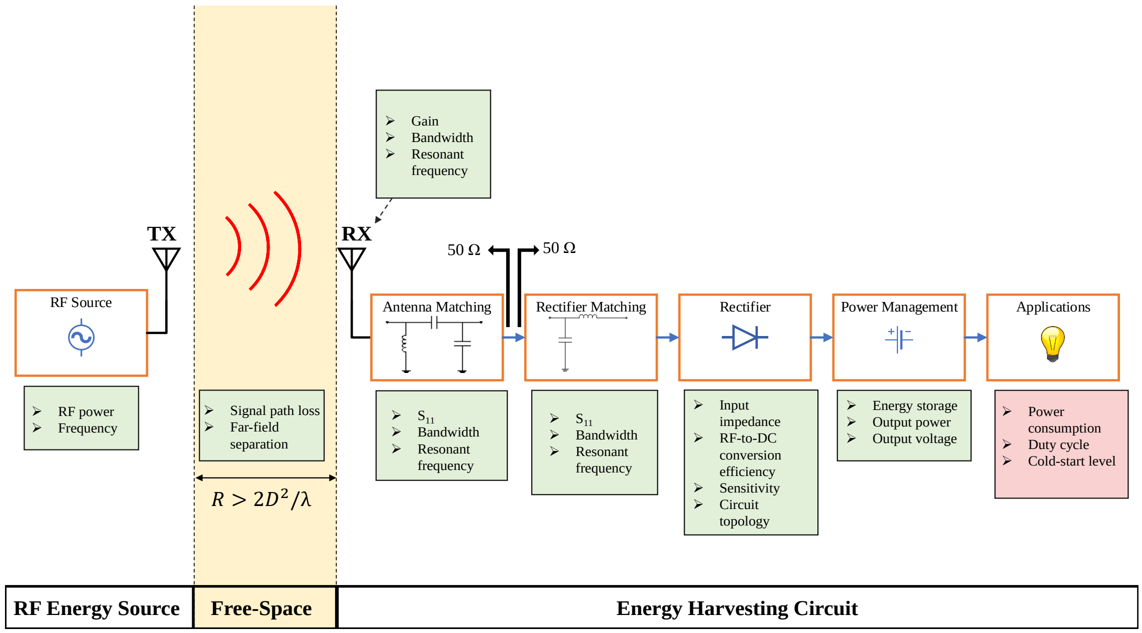

Figure 3: Block diagram of implemented system.

1.4 Current Efforts

Within industry, Powercast Corporation creates various devices powered by far-field RFEH via dedicated power sources [12]. Although their technology also converts RF energy to DC power, their systems operate in the 915 MHz band. On the other hand, our system aims to operate at a higher frequency of 2.45 GHz.

Academic researchers have successfully created devices in an effort to expand the field of RFEH. Many of these devices are designed to operate in common frequency bands which do not require special licenses, such as the 2.4-2.5 GHz WiFi ISM band [13], [14], [15], [16], [17], [18]. However, few of these systems are integrated with a sensor load, and if so, they are not tested at the appropriate power transmit level. For example, in [14], a rectenna sensor network designed at 2.45 GHz is tested using a 10 W Effective Isotropic Radiated Power (EIRP); possible sources operating at this frequency (e.g. routers) typically provide a maximum of 4 W EIRP, the maximum limit set by the U.S. Federal Communications Commission (FCC). While this solution proves the feasibility of integrating a sensor network with rectenna, it does not adequately imitate a practical environment.

Current efforts either:

1. **Omit validation of their system via integration with a practical application**
2. **Lack an accurate sense of how a rectenna-sensor network would fare in realistic conditions**

Figure 4: Rectenna integrated with temperature system operating at 915 MHz [1].

With current research in mind, our project aims to create a rectenna system that operates at 2.45 GHz as an effort towards developing feasible power sources for IoT sensors. Our project will further advancement by not only designing the rectenna system, but also proving it can power commercial, low-power integrated circuits and IoT sensors in a realistic environment. Note that due to technical challenges and time constraints, many simulations and tests are done at the frequency 2.1 GHz (see Section 7.1).

2 Problem Statement & Objectives

2.1 Problem Statement

We aim to design an RFEH system to wirelessly power IoT sensors with a dedicated RF transmitter. An antenna and rectifier system will efficiently convert incoming RF energy into a form able to power a sensor over an arbitrarily long time period.

2.2 Objectives

- Design rectenna for RF-to-DC conversion
- Manufacture and characterize a custom printed circuit board (PCB) for realization of design
- Interface PCB with PMU
- Validate design by wirelessly powering digital temperature sensor

3 Project Plan & Methodology

3.1 Design Approach

The project's design methodology was comprised of a three-phase plan. The first phase consisted of a detailed literature review, along with initial system layout and component selection. The next phase involved simulations of the various sub-components and the integrated system as a whole. The final phase was fabrication and measurement, in which expected simulation results were validated using various RF measurement devices. Table 1 details our project timeline outlining major tasks and the duration over which they were performed.

Fall	
Weeks 1-4	Literature review
Weeks 5-6	Choose antenna, rectifier circuit, diode, load
Weeks 7-10	Simulate rectifier and antenna
Winter	
Weeks 1-3	Finalize rectifier and antenna simulations
Weeks 5-6	PMU integration & load
Weeks 7-10	Layout & fabrication
Spring	
Weeks 1-3	Tune antenna, rectifier, & characterize board performance
Weeks 4-5	Conducted/OTA Measurements, PMU/sensor integration
Weeks 6-7	Compile findings & final report

Table 1: Project schedule & tasks.

3.2 Simulations

Much of this work depends on simulations that approximate the behavior of an RFEH system operating in real-world conditions. Advanced simulation tools are required to characterize the rectifying circuit and design the receive antenna. A non-linear circuit simulator utilizing the Harmonic Balance technique [19] is used to characterize the rectifier network, as the junction capacitance of the diode as well as the physical device properties require careful analysis for efficient matching network design (see Fig. 5). This technique partitions a nonlinear circuit, i.e. a rectifier containing diodes, into non-linear and linear sub-components. The linear subcircuit is analyzed in the frequency domain, while the non-linear subcircuit is analyzed in the time domain, after which the results are Fourier transformed to the frequency domain. The currents through nodes separating the sub-circuits are "balanced" at each harmonic, and from this, the corresponding input impedance can be determined for each frequency contained in the system. This tool was used to quantify the rectifier network's input impedance at the fundamental frequency f_0 and the chosen average input power level. Additionally, this circuit simulator was used to view the generated DC output level in order to estimate RF-to-DC conversion efficiency for various input powers.

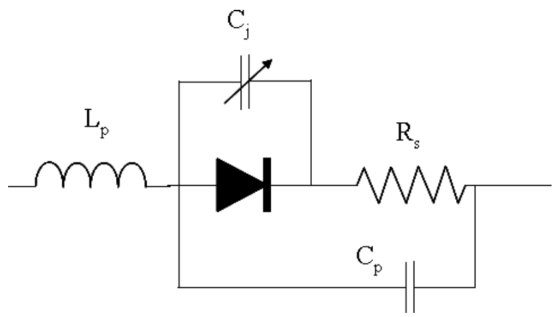

Figure 5: Equivalent circuit of a packaged diode can be analyzed using Harmonic Balance. $\mathrm{L_p}$ is the packaging inductance, $\mathrm{C_p}$ is the packaging capacitance, $\mathrm{R_s}$ is the series junction resistance, $\mathrm{C_j}$ is the junction capacitance [20].

Simulation of the receive antenna took place after the characterization of the rectifier network. This simulation utilized Ansys HFSS, a 3D full-wave electromagnetic solver, in order to accurately design and tune the antenna before fabrication. Once the antenna was fully characterized using numerical tools, the S-parameters of the system were extracted in order to generate a circuit representation of the antenna. This data was then used to simulate the rectifier and antenna in one system. The antenna can be directly matched to the complex conjugate of the input impedance to the rectifier at the fundamental frequency f_0 for a fixed power level P_{in} and load R_{L}. Alternatively, both networks can be matched to a nominal system impedance Z_0. The latter matching method is the approach taken in this design, although the former method may lead to marginally higher power conversion efficiency levels due to lower parasitic component losses.

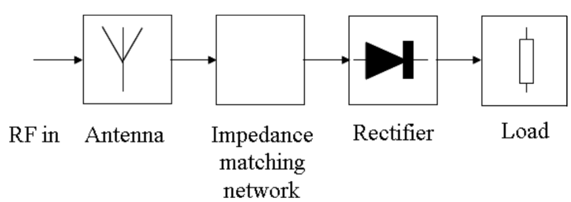

Figure 6: Block diagram of an integrated rectenna system. After the rectifier/load network has the input impedance characterized for a specific RF power input, an impedance matching network can be designed and placed between the antenna and rectifier [20].

4 System Components

This section will cover the design, simulation, and measurements of each individual component in the finalized RFEH system.

4.1 Antenna

The receive antenna was designed to both capture incident power densities and present an input impedance close to the system impedance Z_0 at the design frequency f_0. Many different antenna topologies can be utilized in RFEH systems, however, with one of the primary system objectives being a low-profile geometry, a planar microstrip based antenna was selected as the antenna type. Microstrip antennas have a simple initial design process, which can then be tuned to achieve certain performance results such as polarization diversity or dual-band operation [11]. Additionally, microstrip antennas can utilize various feed networks, allowing for various system layout configurations, and can be efficiently integrated onto a PCB sharing analog and digital circuitry.

4.1.1 Planar Inverted-F Antenna

The antenna topology chosen for the final design was the **planar inverted F antenna** (PIFA). The PIFA consists of a rectangular planar element placed above a ground plane, a short-circuit pin, and a microstrip feed. The PIFA layout used in HFSS simulations is depicted in Fig. 7.

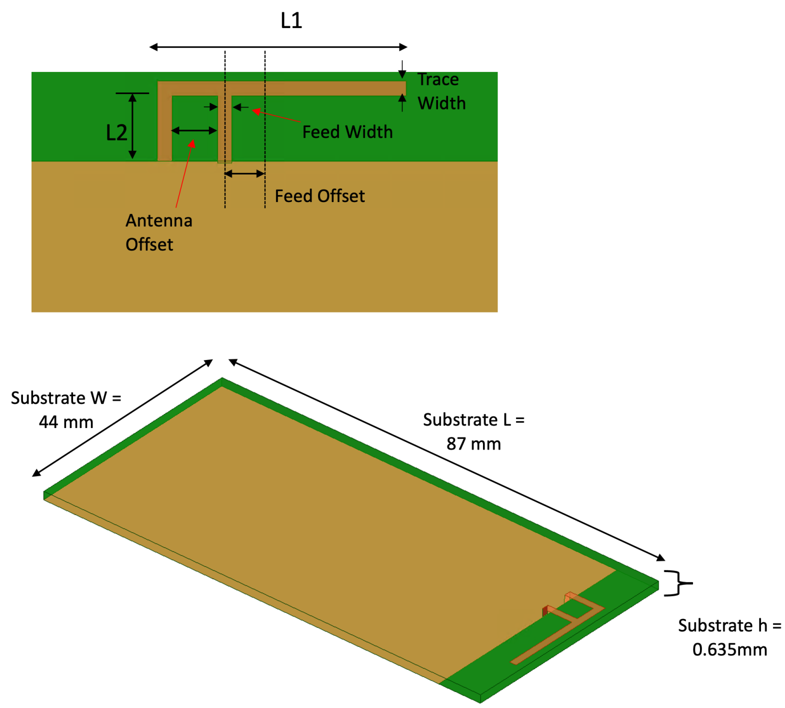

Figure 7: PIFA geometry and PCB dimensions.

The PIFA is a variant of a standard monopole antenna, where the top section has been folded to be parallel to the ground plane, effectively creating the image of a dipole. This also reduces overall antenna height while maintaining a length required for resonance. The arm denoted by length L_1 forms a shunt capacitance to ground, which is inductively tuned by the short-circuit stub of length L_2.

The ground plane plays a crucial role in the operation of the PIFA. Exciting currents in the PIFA causes excitation of currents in the ground plane. The radiated electromagnetic field is a result of the interaction between the PIFA and its image below the ground plane. The radiation performance is dependent on the geometry of the ground plane, and is typically enhanced when the ground plane is much greater than the dimensions of the antenna itself. In general, the width of the ground plane should be at least as wide as the PIFA L_1 arm, while the length should be at least $\lambda/4$ in height [11], where λ is the free-space wavelength at the operating frequency.

The dimensions of the PIFA are listed in Table 2. The resonant frequency of the antenna is determined by the lengths of the radiating arm, shorting pin, and trace width, and the location of the feed relative to the shorting pin [11]. The resonant frequency is specified such that $L_1 + L_2 + (\text{Trace Width}) = \lambda/4$ at f_0. In this case, λ is the free-space wavelength at f_0. These values are fine-tuned using the Optometrics tool in HFSS to get an optimal resonant behavior at f_0. The initial design frequency used in all the simulations is $f_0 = 2.45$ GHz, however this value can be adjusted by means of a matching network (i.e. $f_0 = 2.1$ GHz), as it is for the final system implementation discussed in later sections.

L1 mm	**L2** mm	**Ant. Offset** mm	**Feed Offset** mm	**Feed Width** mm	**Trace Width** mm
22.5	8.47	3.9	4.5	1.2	1.3

Table 2: Optimized PIFA dimensions.

The numerically tuned antenna is simulated in HFSS to characterize its directivity and efficiency, as measuring these parameters in a lab requires extremely specialized equipment and highly controlled test environments which were not accessible for this project. As seen in Fig. 8, the gain of the antenna is fairly omnidirectional with a peak gain of 3.7 dBi. This gain value is used in theoretical link-budget calculations involving the fabricated design as this parameter was not able to be characterized without an anechoic chamber.

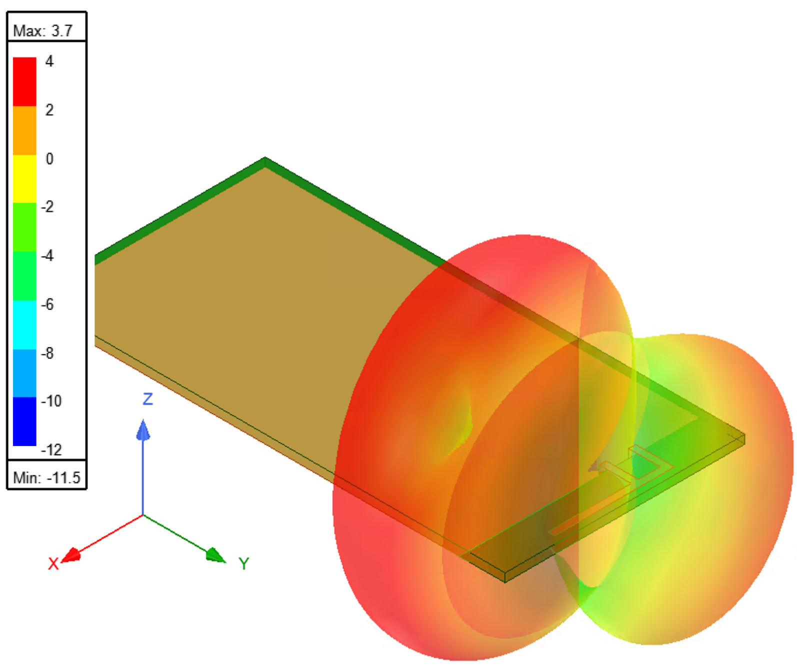

Figure 8: Simulated PIFA gain pattern.

The measured PIFA is tuned to an operational frequency of $f_0 = 2.1$ GHz by means of a π-topology matching network. The lumped component values along with the reflection coefficient S_{11} response of the system is depicted in Fig. 9.

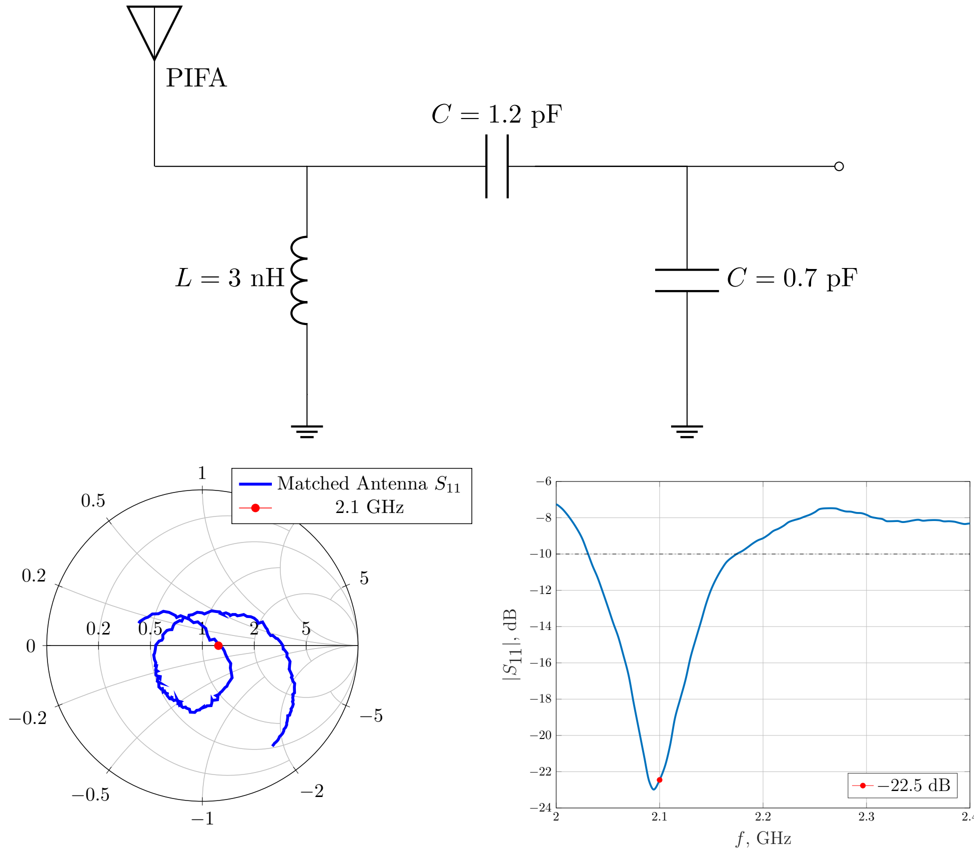

Figure 9: Antenna matching network (top) and S_{11} response depicted by Smith chart (bottom left) and log-magnitude plot (bottom right).

4.2 Rectifier

The rectifier is responsible for converting an input AC signal to a DC output that can then be used to power application-specific loads. In order to ensure maximum power transfer between the antenna and rectifier, reflection should be reduced and the rectifier should be matched to the system impedance, i.e. $Z_0 = 50\ \Omega$. A voltage doubler circuit, shown in Fig. 10, and an input power of -10 dBm were chosen based on their prevalence in RFEH literature [1], [21], [16], [14]. Here, Z_{source} denotes where the matching network will be placed, which is implemented to match the fundamental frequency's input impedance to the nominal system impedance Z_0 for a specific input power and load resistance.

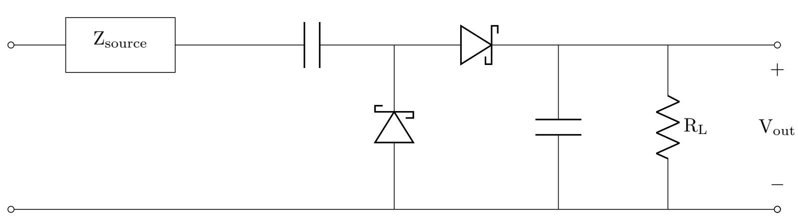

Figure 10: Grenaicher voltage doubler circuit consisting of Schottky diodes, capacitors, and load resistance.

The rectifier's impedance was analyzed using large-signal s-parameter (LSSP) simulations and Harmonic Balance solvers in ADS software. The rectifier circuit is matched at 2.1 GHz, with matching components obtained through ADS optimization and physical tuning (see Fig. 11 for component values and Fig. 18 for S_{11} response).

Due to the non-linear nature of the diode, the rectifier performs differently as the input power and load resistance vary. The effects of input power and load resistance on efficiency are visualized in Fig. 12. The graph shows that a maximum efficiency of 30% occurs with input powers between -5 to -0 dBm, with a load resistance less than 5 kΩ. Ideally, the rectifier would operate in this region of maximum efficiency.

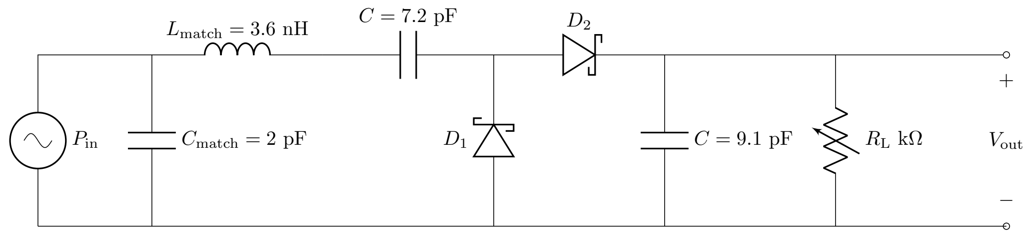

Figure 11: Matched rectifier circuit with variable input power and output load control.

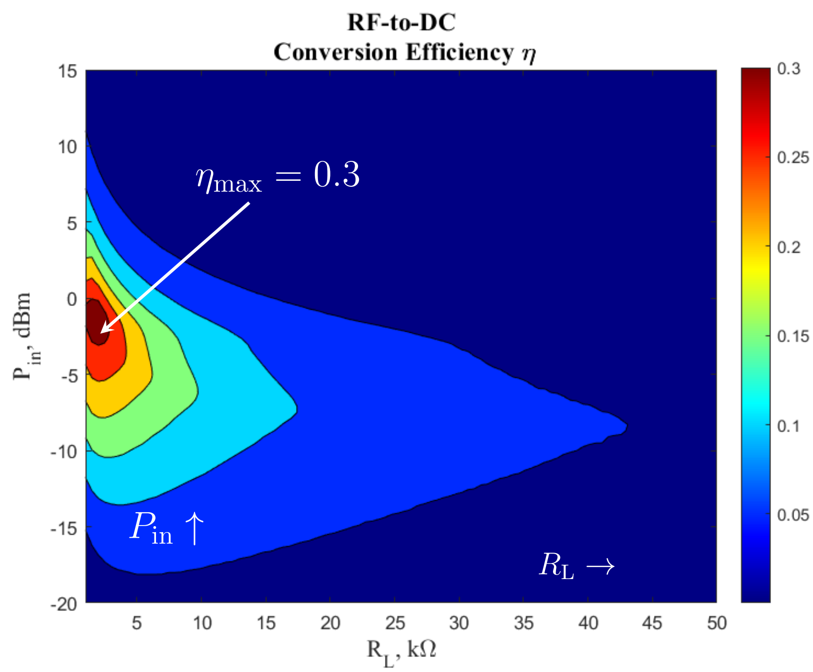

Figure 12: Simulated contours of efficiency as a function of load resistance and input power.

4.3 PCB Layout

The designed antenna and rectifier elements detailed in the previous sections were integrated onto a common PCB substrate and fabricated in order to conduct system-level tests and validate the design concept. Altium designer was used for both the schematic capture and PCB layout of the design (see Fig. 13 and 15). As seen in Fig. 14, the fabricated PCB area is confined by the dimensions used to simulate the PIFA antenna in HFSS (refer to Fig. 7).

Lumped components, i.e. Murata GCM15 capacitor and LQW15 inductor, synthesized the matching networks and rectifier. These components are rated for radio-frequency operation and have high component Q-factors, leading to minimal component losses and thus enhancing power conversion efficiency [22]. The diodes used in the rectifier are the SMS7630-040LF by Skyworks [23]. This particular series is a Schottky diode, which is essential for RFEH applications as they have the lowest turn-on voltage, are self-biasing, and have fast switching speeds. Additionally, this diode was selected due to its low junction capacitance of $C_{j0} = 0.14$ pF, relatively low parasitic series resistance of $R_s = 20\ \Omega$, and minimal packaging parasitic inductance and capacitance.

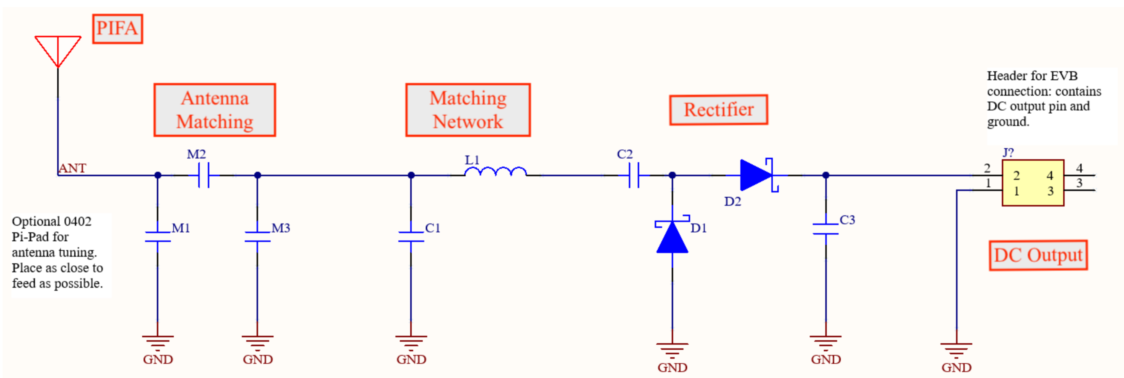

Figure 13: Custom rectenna schematic; designed in Altium.

Via shielding was added to enhance isolation between the antenna and rectifier, as well as to reduce parasitic inductance on the board. From a measurement standpoint, a top-layer ground is required in order to have a properly grounded RF probe connected to the PCB for characterization. Table 3 details the substrate parameters of the board. The board uses Rogers 6006 dielectric [24], which was chosen based on its permittivity and substrate height such that trace widths of characteristic impedance $Z_0 = 50\ \Omega$ can smoothly interface with 0402 surface mount components, thereby minimizing parasitic stub effects on the board. Additionally, this substrate is very low loss and has consistent material properties, resulting in designs that more accurately reflect the simulations.

At the output of the rectifier are additional solder pads for connecting a 1×2, 1.27 mm pitch header in order to interface with a standalone PCB containing the power management IC and digital temperature sensor.

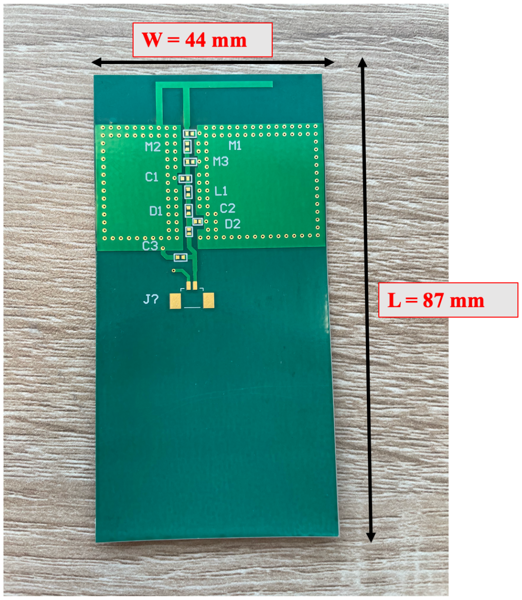

Figure 14: Fabricated PCB.

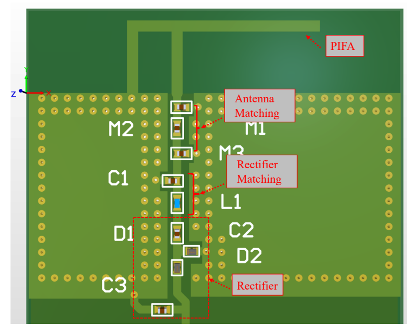

Figure 15: PCB layout done in Altium.

Substrate	**Permittivity** ϵ_r	**Dielectric Height** h	**Trace Width** w
Rogers 6006	6.15	0.635 mm	0.935 mm

Table 3: Substrate specifications.

5 System Performance Analysis

In this section, the measured performance of the system is presented. First, the rectifier is characterized by soldering a 50 Ω probe directly to the rectifier and its matching network in order to control the power supplied to the circuit. Multiple experiments are run in this way to characterize the rectifier to observe how its behavior aligns with ADS simulations. Next, over-the-air (OTA) testing is performed utilizing the receive antenna as well as a dedicated RF power source. The rectified output voltage is characterized as a function of incident power density, and theoretical link-budgets are carried out to model the transmitter-to-receiver path loss.

5.1 Rectifier Testing

Extensive testing of the fabricated rectifier board was carried out in order to validate the physical PCB against the simulated expectations. The first test carried out was a measurement of the rectifier's input impedance at the fundamental frequency f_0 when presenting a 50 Ω source impedance to the circuit. The simulated and measured results of the rectifier with $R_L = 10$ kΩ and $P_{in} = -10$ dBm are plotted on a Smith Chart in Fig. 16. Both simulation and measurement align well, indicating that the simulation model of the board and components is robust.

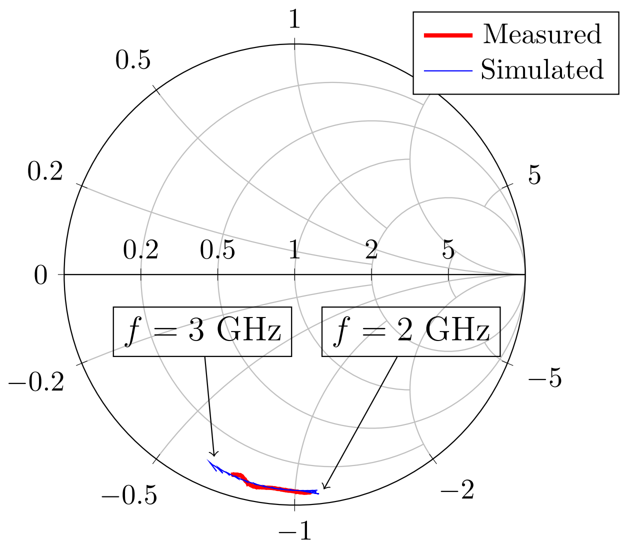

Figure 16: Smith Chart plotting simulated and measured results of the unmatched rectifier from 2 to 3 GHz.

For designing/verifying the performance of the rectifier's matching network and power conversion efficiency, the board was modified as shown in Fig. 17. A $50\ \Omega$ RF probe was soldered to the top ground of the PCB to connect a VNA or RF signal generator in order to directly interface with the rectifier.

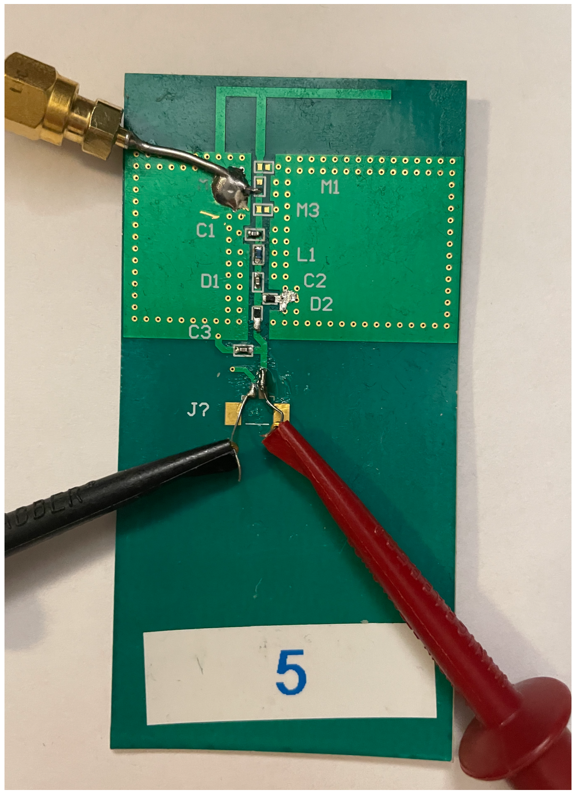

Figure 17: Test setup for matching rectifier and characterizing the conducted response. A $50\ \Omega$ RF probe is soldered to the top ground of the PCB. This is used to interface with a vector network analyzer or signal generator depending on the test.

Using the measured input impedance data along with ADS optimizations of matching network topologies, a suitable matching network is designed for a fundamental frequency of $f_0 = 2.1$ GHz. The resulting matching circuit topology and lumped element values along with the S_{11} response is shown in Fig. 18.

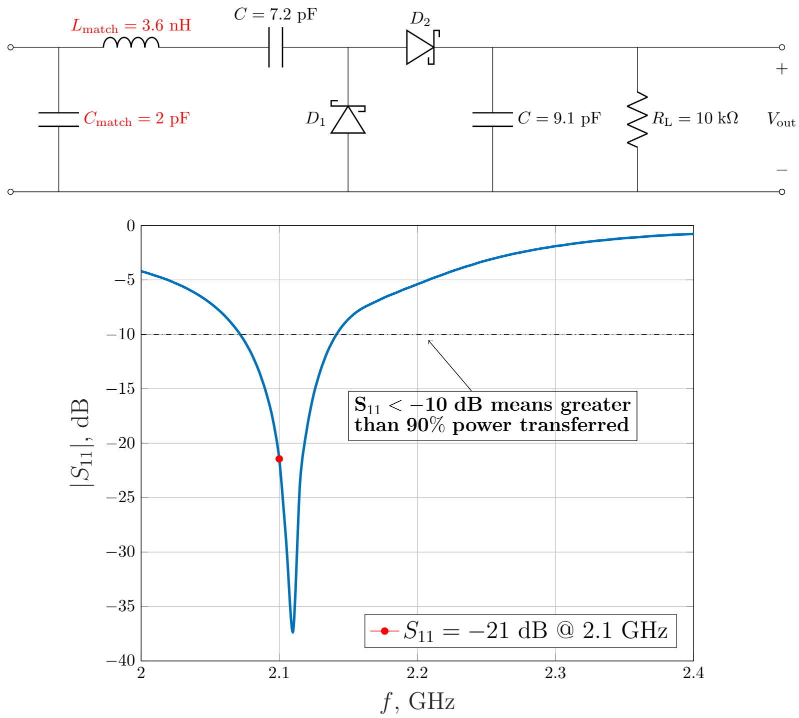

Figure 18: Matched rectifier circuit (top) and S_{11} response for fixed input power $P_{\text{in}} = -10$ dBm, $R_{\text{L}} = 10$ kΩ (bottom).

After successfully matching the rectifier on the PCB, the output voltage is characterized as a function of load resistance for different input powers. The test setup consists of an RF signal generator to control the input power and frequency, the rectifier, jumpers to a breadboard, a potentiometer to control the load resistance, and a digital multi-meter to record output voltage levels. The setup is shown in the top of Fig. 19.

The bottom of Fig. 19 shows the simulated and measured output voltage versus load resistance at different power levels. From the plots, it is clear that the physical board aligns closely with the simulations. Analyzing the trends of these curves, one can see that, for low load resistances below 3 kΩ, low output voltages are produced. This is important when integrating with the PMU, as the IC must present an effective DC load resistance high enough to ensure that operation conditions are satisfied. It is also observed from the curves that above a certain value, increased load resistance does not result in higher output voltage levels.

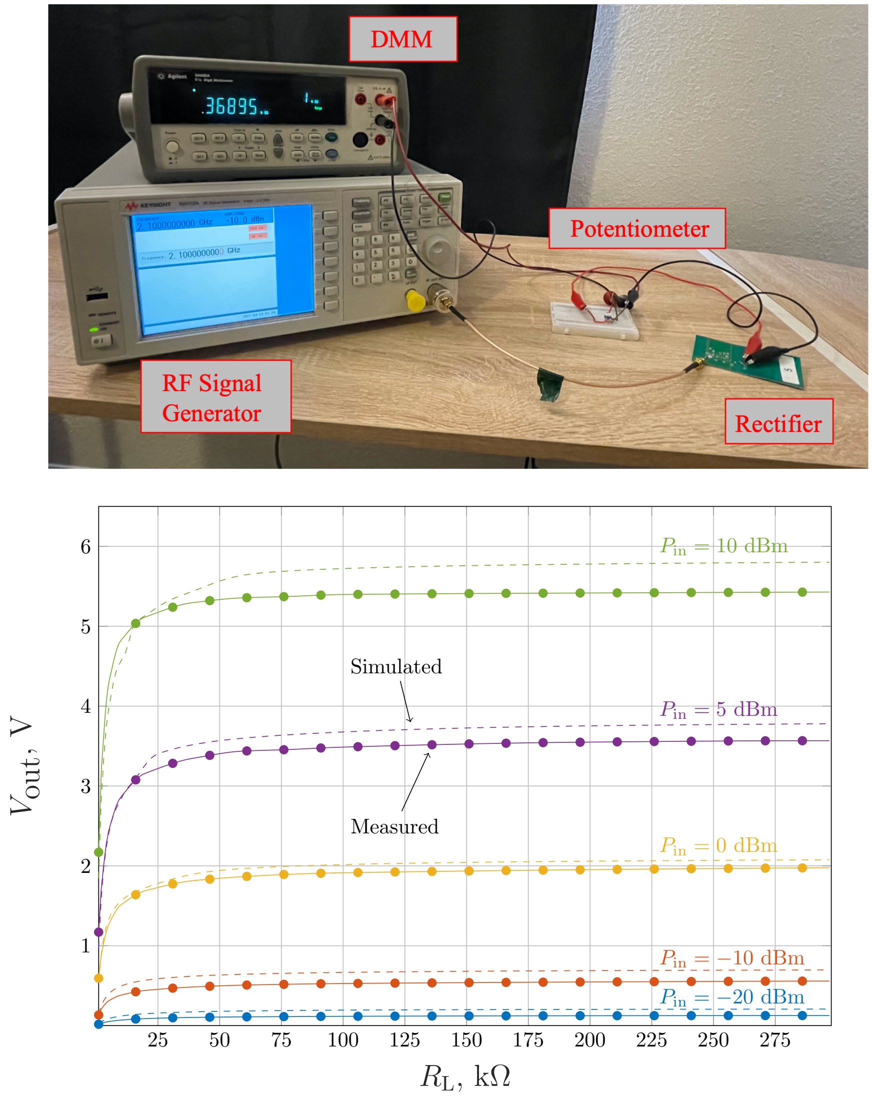

Figure 19: Test setup for characterizing the rectifier (top) and output voltage V_{out} as a function of load resistance R_{L} for different input powers P_{in}.

Finally, we characterize the power conversion efficiency η_{PCE}. The power conversion efficiency is defined as the amount of DC output power P_{DC} attained with respect to the RF input power P_{in},

$$\eta_{\text{PCE}} = \frac{P_{\text{DC}}}{P_{\text{in}}} = \frac{V_{\text{out}}^2}{R_{\text{L}} \cdot P_{\text{in}}} \tag{2}$$

We observe general agreement between the behavior of simulation and measurement, however our measurements likely have increased component losses, leading to lower overall efficiency as seen in Fig. 20.

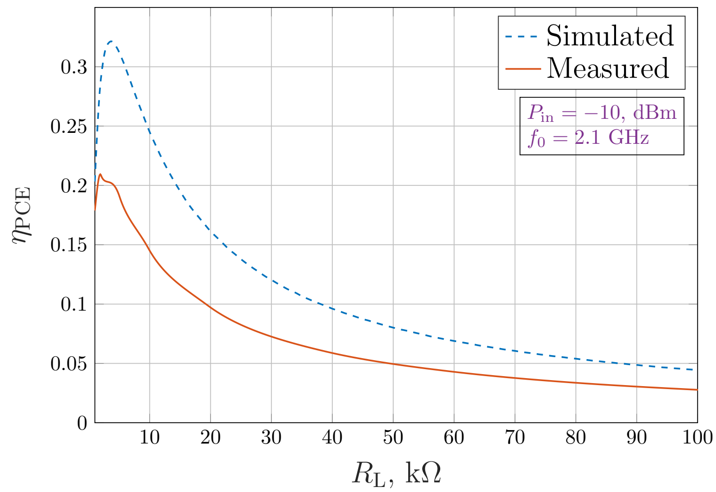

Figure 20: Simulated and measured power conversion efficiency as a function of load resistance R_{L} for a fixed input power $P_{\text{in}} = -10$ dBm and frequency $f_0 = 2.1$ GHz

5.2 Over-the-Air Testing

After independently validating the performance of the rectifier and antenna, the next set of experiments considered the integrated antenna and rectifier's ability to rectify RF signals captured OTA from a dedicated RF transmitter.

The system performance depends critically on the line-of-sight between the transmitter and receiver, how well-matched each is to its system impedance, the respective gain of each element, and the field polarization of the antenna, which dictates the types of fields an antenna transmits and receives.

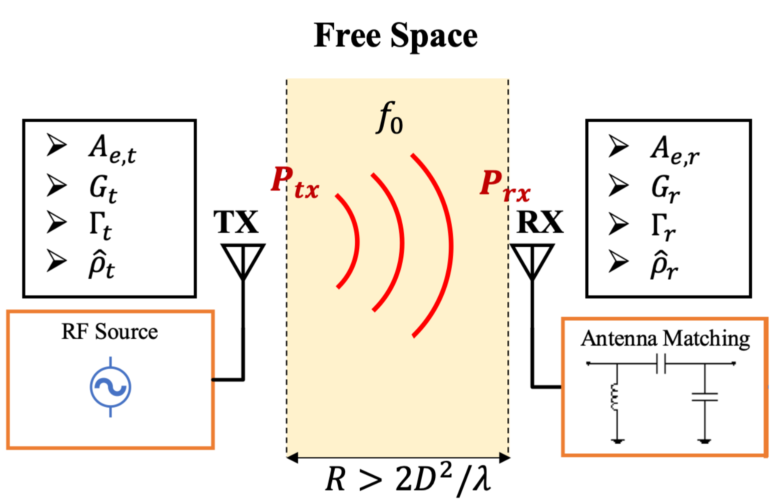

Figure 21: Transmit and receive block diagram and associated variables that affect over-the-air RFEH system performance.

Device	Effective Aperture A_e	Gain G	Reflection Coefficient Γ	Polarization $\hat{\rho}$	Max Linear Dimension D
TX	513.6 cm^2	15 dBi	< -15 dB	Linear: vertical	20.6 cm
RX	38.1 cm^2	3.7 dBi	< -15 dB	Linear: horizontal/vertical	2.5 cm

Table 4: Test setup performance parameters used for theoretical link-budget analysis.

Table 4 lists important parameters used for calculating the transmitter-to-receiver link budget based on the Friis equation given in (1). The received power versus distance from the transmitter for a source power $P_t = 13$ dBm and frequency $f_0 = 2.1$ GHz is plotted in Fig. 22.

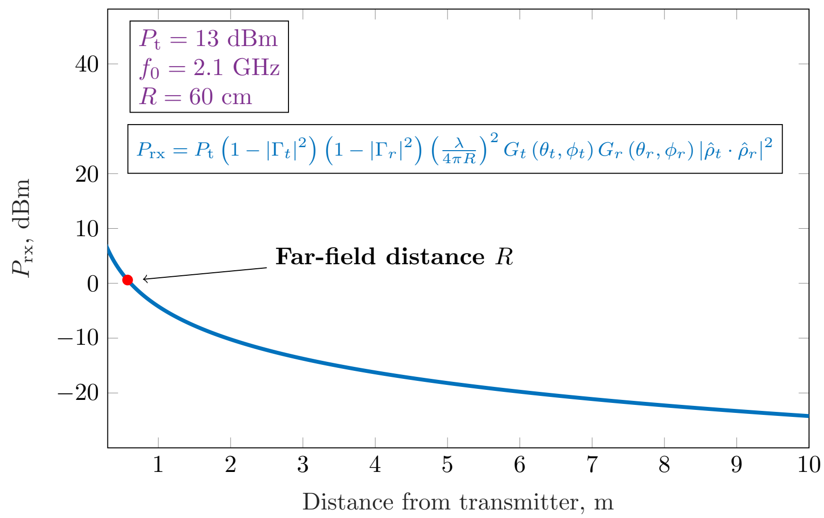

Figure 22: Received power as a function of distance from the transmitter. The received power is calculated based on the Friis equation boxed in blue for a fixed test setup using the parameters in purple along with values from Table 4.

With an understanding of the received power levels able to be captured in the test setup, measurements are taken in order to characterize the system performance. The OTA measurement setup is shown in Fig. 23. The setup consists of an RF signal generator, a power amplifier, a power supply for DC biasing, a high-gain transmit antenna, the rectenna, a potentiometer, and a digital multi-meter. The power amplifier is used to slightly exceed the maximum output power of the RF signal generator. Note that in this test setup, the peak EIRP of the transmitter is 27 dBm.

The resulting output voltage versus load resistance for different incident power densities S_i is shown in Fig. 24. This curve follows the same trend shown in the conducted mode output voltage measurements (see Fig. 19). The green curve represents the output voltage for the maximum incident power density able to be achieved for a transmitter-to-receiver separation distance equal to the far-field distance of about 62 cm.

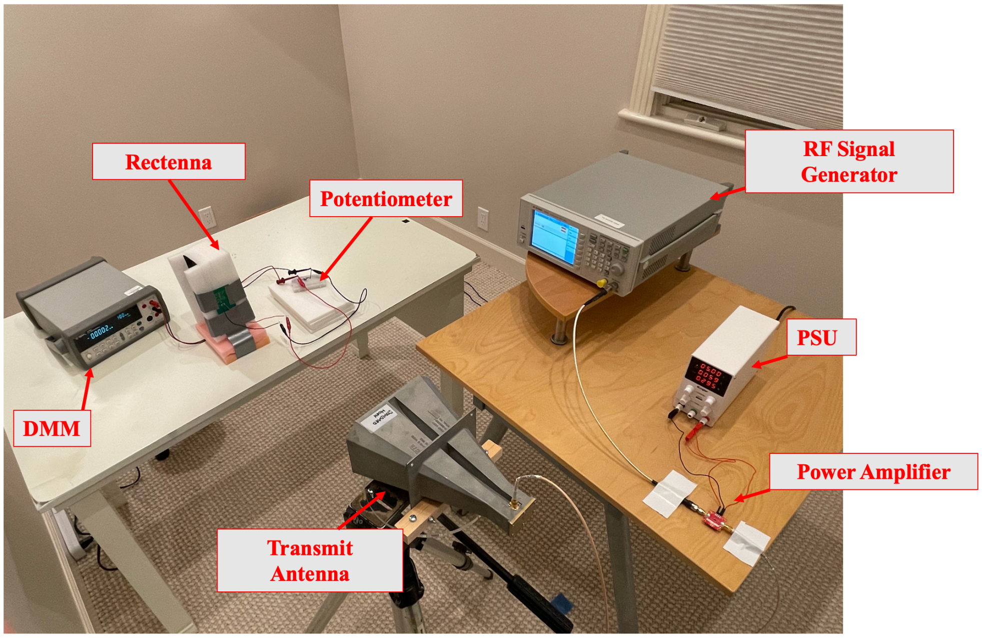

Figure 23: OTA system characterization test setup.

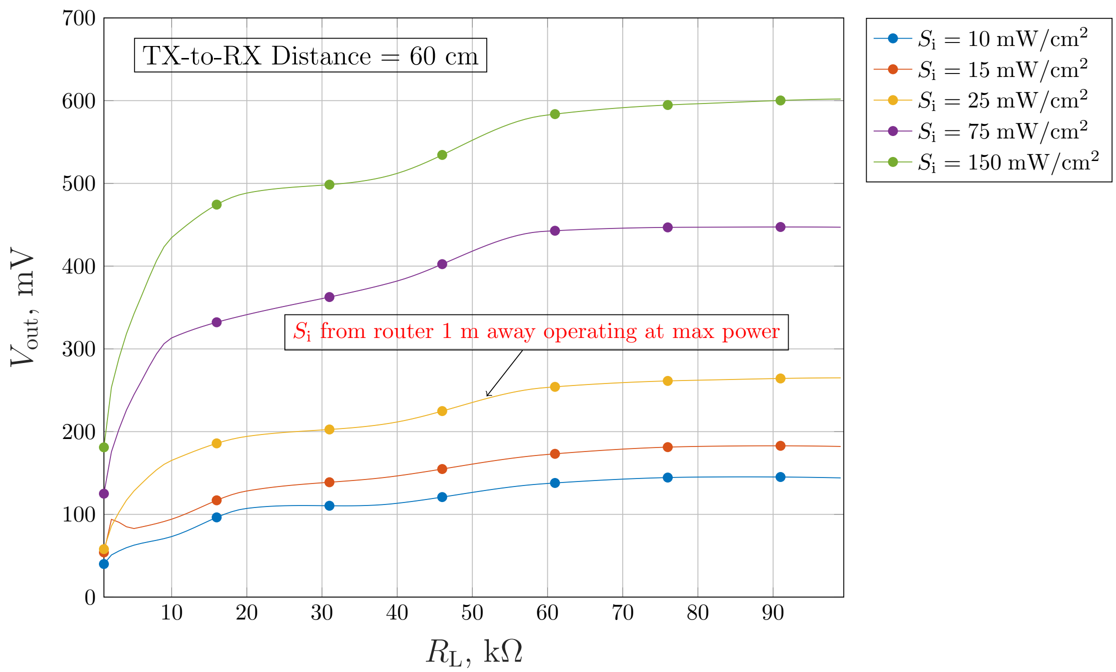

Figure 24: Output voltage V_{out} vs. load resistance R_{L} for different incident power densities S_i. The orange curve corresponds to an approximate incident power density one would observe standing 1 m away from a router transmitting at a max EIRP of 36 dBm.

6 Application: Wirelessly Powered Temperature Sensor

Our selected application is to power a temperature sensor using the designed rectenna system.

6.1 Operation & Block Diagram

Figure 25 abstracts the sensor load in block diagram format. The sensor load consists of a commercially-available PMU, rechargeable battery, microcontroller (MCU), and sensor.

The PMU selected was the TIBQ25570, which functions as a boost charger for the battery and hosts a maximum power point tracking feature (MPPT) [25]. The MPPT tries to optimize the power extraction process, and in doing so, indirectly modulates the input impedance. From the PMU, the battery can be charged and is then used to power the MCU and sensor. The MCU collects data from the sensor, and sends it to the computer via a serial port. The MCU (MSP430FR5969 Launchpad Development Kit) was designed for low power operation, with multiple communication protocols including I2C, UART, and SPI [26]. The temperature sensor, TMP116, is a digital, low-powered sensor with SMBUS- and I2C-compatible interfaces [27]. See Table 5 for load application specifications.

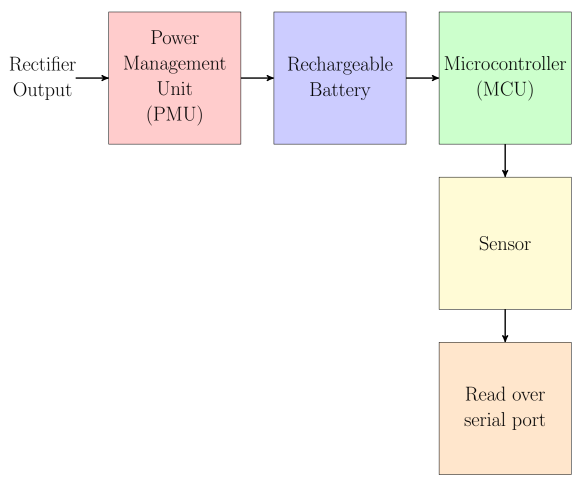

Figure 25: Block diagram of sensor load.

	PMU	MCU	Sensor
Min. Cold Start (V)	0.6	–	–
Min. Operation (V)	0.1	1.8	1.9

Table 5: Specifications for sensor load.

6.2 OTA Integrated Rectenna and Sensor Load Testing

In our final validation, the entire integrated system was examined. The test setup, shown in Fig. 26, is similar to Section 5.2, with a horn antenna as the transmitter and the rectenna as the receiver connected to the sensor load.

The test was conducted over 8 hours with the transmitter remotely powering the sensor, with success deemed when data was logged. Fig. 27 shows results comparing our rectenna and sensor load to only the sensor load, which was solely powered by battery. The battery-powered sensor load only lasted for 2 hours (red curve), while the rectenna charged the sensor load for the entire 8 hours (blue curve).

Based on this test, our rectenna system was able to successfully charge the sensor load for an extended period of time. However, the rectenna system was unable to overcome the PMU's cold-start mode due to the fact that the rectifier was designed for a 10 kΩ static load, which does not accurately reflect the PMU's varying impedance as a result of its MPPT feature. Nevertheless, we were still able to demonstrate that the rectenna system works in a steady state operational mode.

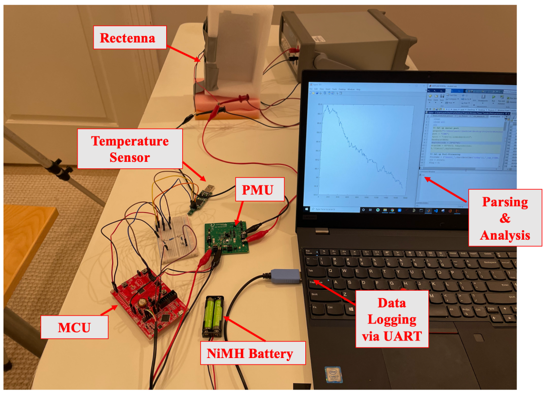

Figure 26: Rectenna with sensor load.

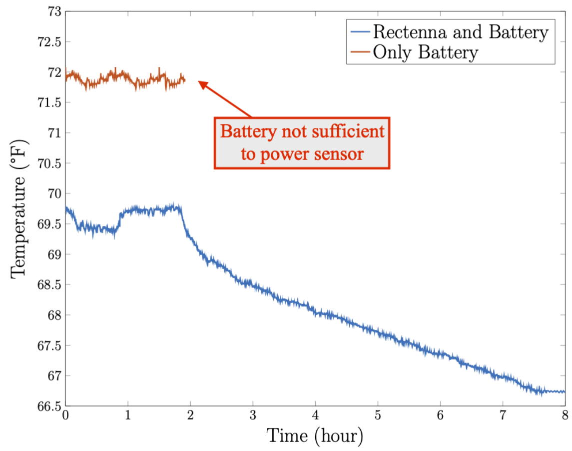

Figure 27: OTA test with sensor load vs. only sensor load over 8 hours.

7 Project Assessment

7.1 Design Changes

In the course of system bring-up, tuning, and preliminary system-level tests, it was found to be difficult to synthesize a matching network with the rectifier at the original design frequency of $f_0 = 2.45$ GHz. Matching a rectifier to the system impedance Z_0 is difficult as the rectifier input impedance at f_0 will vary depending on load conditions and input power. Effectively, when a matching network is synthesized for one particular impedance measurement, the input power to the rectifier increases. This leads to a change of input impedance of the rectifier due to the non-linear response of the diodes, and results in the rectifier not being matched again.

To help deal with this issue, the circuit model of the PCB, traces, and vendor lumped element models were prototyped in ADS in order to gain an understanding of how the circuit changes as a function of these parameter values, as well as the relative input power P_{in} and DC load resistance R_{L}. Utilizing the Harmonic Balance simulator in conjunction with the optimization controller led to close agreement between the raw input impedance measurement to the rectifier for both the measured and simulated response as is seen in Fig. 16.

Despite the agreement between the raw input impedance measurements of the model and PCB, synthesizing a matching network based on ADS optimization was not initially able to be accomplished at $f_0 = 2.45$ GHz. However, it was found that shifting to a slightly lower frequency of $f_0 = 2.1$ GHz was able to produce a solid matching network that was reliably measured on multiple boards. In the interest of time, this matching network was implemented on all of the PCB variants in order to conduct system-level tests of the design. Additionally, the antenna was simply re-matched to this frequency using the extra π-topology pads included on the PCB.

The initial antenna characterization was validated against the raw simulation model using the original design frequency of $f_0 = 2.45$ GHz. The simulated, measured, and matched S_{11} responses for this design frequency are shown in Fig. 28.

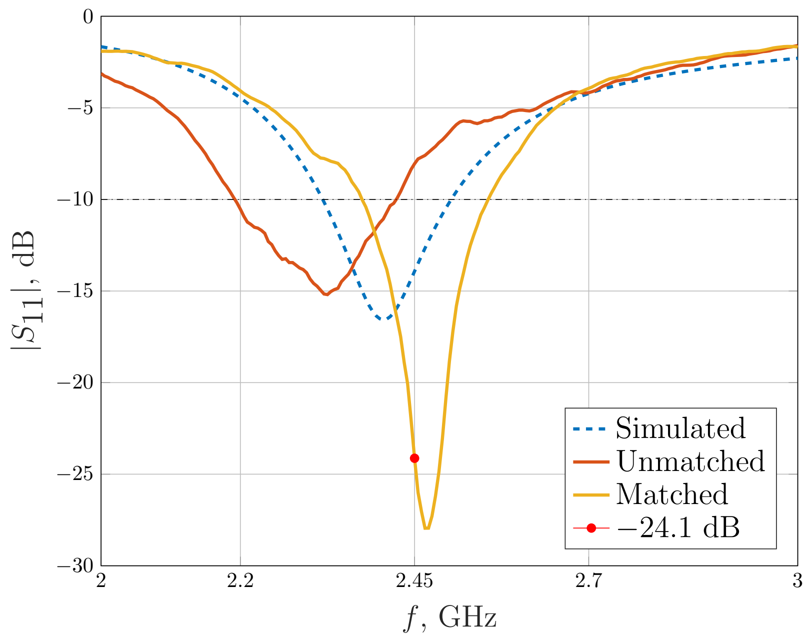

Figure 28: Simulated, measured, and matched S_{11} of PIFA antenna at original design frequency $f_0 = 2.45$ GHz.

After system-level tests using the new frequency of $f_0 = 2.1$ GHz, it was observed that switching to a higher frequency rated component library was able to produce an acceptable rectifier matching level at 2.45 GHz (refer to Table 6). Lumped components have a self-resonant frequency (SRF), which helps to characterize their parasitic behavior. In essence, an inductor acts like an inductor up to its SRF, and likewise for a capacitor. When the component operates in a region above its SRF, then its parasitic behavior will affect performance.

The synthesized matching network along with the S_{11} response is shown in Fig. 29. Once again, in the interest of time, this network was not implemented for system-level testing. However, further work on this project should use this matching circuit as the operation at 2.45 GHz is in the FCC unlicensed ISM band [28].

Element	Series	Value	SRF
Rectifier Matched at 2.1 GHz			
Capacitor	Murata GCM15	2 pF	2 GHz
Inductor	Murata LQW15	3.6 nH	11 GHz
Rectifier Matched at 2.45 GHz			
Capacitor	AVX Accu-P	2.7 pF	4.5 GHz [29]
Inductor	Coilcraft 0402CS	2.2 nH	10.8 GHz [30]

Table 6: SRF Comparison of matching components between the rectifier matched at 2.1 GHz versus 2.45 GHz.

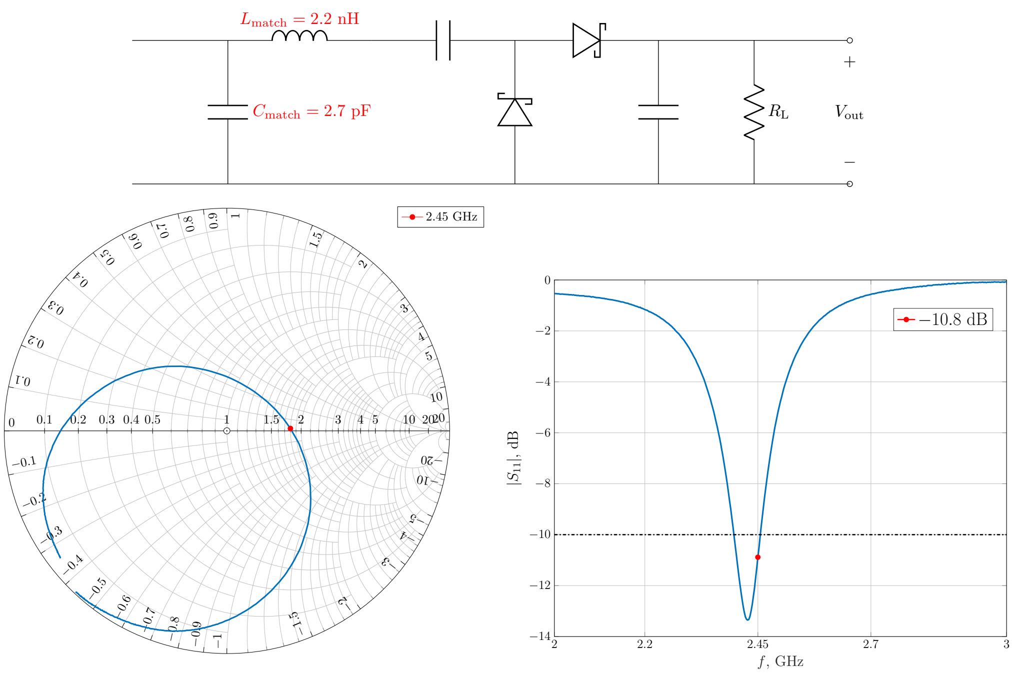

Figure 29: $f_0 = 2.45$ GHz rectifier matching network (top), Smith Chart (bottom left), and log-magnitude response (bottom right).

7.2 Performance Assessment

An assessment of project performance has been summarized in Table 7. All objectives have been completed in their entirety or in some capacity.

The rectifier and antenna were successfully designed and fabricated. The rectenna can perform RF-to-DC conversion by receiving RF energy and converting it to DC power. In addition, the system has been measured and validated, with simulations and measurements demonstrating good alignment.

Initially, we were unable to implement a rectifier matching network at 2.45 GHz, but were able to match the rectifier at 2.1 GHz and conduct our tests at this frequency. Later, we realized that the lumped components needed higher SRF, and were able to match the rectifier at 2.45 GHz.

The rectenna was integrated with the sensor load, but does not reliably operate in cold-start mode due to the fact that the PMU impedance greatly varies as a result of its MPPT feature. Essentially, the PMU modulates its impedance based on the rectifier's output voltage, but the rectifier changes its impedance based on the load, which includes the PMU.

However, system performance was validated in steady state operational mode, successfully proving that our RFEH system is capable of charging a battery and sustaining sensor operation for an extended period of time (8 hours).

Objectives	**Status**	**Source of Error**
Design rectifier and antenna for RF-to-DC conversion	✓	–
Layout PCB, fabricate PCB, and tune antenna	✓	–
Implement matching networks	Antenna is well-matched; rectifier could not initially be matched for 2.45 GHz	Needed components with higher SRF
Measure and validate	✓	–
Integrate rectenna with sensor load	Yes, but cannot reliably operate in cold-start mode	PMU input impedance differed from expected ($R_L = 10\ \text{k}\Omega$); Varies depending on PMU state

Table 7: Assessment of our RFEH system with sensor load.

8 Professional Issues & Constraints

This section examines our project from a professional lens, namely, analyzing its reliability and ethical implications.

8.1 Reliability & Sustainability

Our system is working towards creating more sustainable technology by providing an alternative, energy-efficient power source. Dedicated RFEH is especially suitable for applications where the sensor is difficult to access, or the batteries need to be frequently replaced. By providing a method to efficiently charge batteries via WPT, we intend to lay the groundwork for IoT technology that minimizes environmental waste. Additionally, standard materials and components were used (e.g. PCB substrate, lumped components, diodes, off-the-shelf sensor), making the designed system easy to manufacture and reproduce for economic sustainability.

However, performance may negatively be affected by factors including parasitics and manufacturing process variations. Moreover, the rectifier is challenging to design as performance depends on the input power and load impedance. The storage element must also be carefully selected such that it discharges slower than the charging rate of the rectenna and PMU.

8.2 Ethical Considerations

There are a few possible misuses of this technology. Firstly, the rectenna system is designed to operate at very low powers, potentially advancing the development of low-profile devices used to monitor people and gather data. Secondly, certain environments housing these sensors could be vulnerable to cybersecurity attacks or other electromagnetic disruptions which could intentionally cause system malfunctions. Users with bio-medical implants relying on RFEH could be especially vulnerable to such risks. Although this technology strives to minimize the damage on the environment from an increasing usage of IoT devices, there is the possibility that bad actors will exploit this technological development to power technologies with nefarious intent.

8.3 Methods of Improvement

In this section, we cite a few ways that researchers have found to improve performance. First, custom energy harvesting ICs can be designed to efficiently interface with the rectenna and selected load [31]. This differs from our designed system where a commercially-available energy harvesting module was used. Secondly, techniques involving multi-path energy routing, such as using a relay node in between the transmitter and receiver, have been shown to improve performance, especially over long distances [32]. Lastly, transmit signals with high peak-to-average power ratios (PAPR) can yield higher RF-to-DC conversion efficiency, compared to the single carrier signals used in our tests [33].

9 Conclusion & Future Work

The goal of this project was to display the validity of RFEH by designing and validating our own custom solution capable of powering an IoT sensor. This work was motivated by an increasing reliance on IoT devices, and thus, a demand for more power to be delivered in an efficient and sustainable fashion. In doing so, robust simulations were conducted using powerful solvers and modern techniques such as ADS and HFSS. The design was then laid out and fabricated. Extensive tests in different conditions validated our system and provided proof of the system's ability to power a commercial IoT temperature sensor. Assessing our performance, original objectives were achieved and when faced with technical challenges, the project was appropriately adapted in a manner that successfully validated our system.

We have outlined a few tasks to further improve our design:

1. Performing electromagnetic co-simulation of the PCB with lumped components and diode models, thereby providing a comprehensive simulation that accounts for component and trace parasitics
2. Integrating the PMU and sensor load onto the remaining PCB area to create a compact and comprehensive system
3. Analyzing the fabricated antenna in an anechoic chamber for OTA characterization
4. Exploring input signal optimization to improve RF-to-DC conversion efficiency.

Overall, this project has demonstrated many of the exciting and emerging applications of RFEH, and has served to open innovation for future researchers.

References

[1] S. Nikoletseas, Y. Yang, and A. Georgiadis, *Wireless Power Transfer Algorithms, Technologies and Applications in Ad Hoc Communication Networks*. Gewerbestrasse 11, 6330 Cham, Switzerland: Springer International Publishing AG, 2016.

[2] N. Tesla, "The transmission of electrical energy without wires as a means for furthering peace," *Electrical World and Engineer*, p. 21–24, 1905.

[3] J. Koomey, S. Berard, M. Sanchez, and H. Wong, "Implications of historical trends in the electrical efficiency of computing," *IEEE Annals of the History of Computing*, vol. 33, no. 3, pp. 46–54, 2011.

[4] T. Jury, "How many iot devices are there in 2020?" [Online]. Available: https://techjury.net/blog/how-many-iot-devices-are-there/

[5] W. C. Brown, "Microwave to dc converter," U.S. Patent 3434678A, May. 1969.

[6] S. Keyrouz, "Practical rectennas, rf power harvesting and transport," Ph.D. dissertation, Eindhoven University of Technology, Eindhoven, The Netherlands, 2014.

[7] T. Paing, J. Morroni, A. Dolgov, J. Shin, J. Brannan, R. Zane, and Z. Popovic, "Wirelessly-powered wireless sensor platform," in *2007 European Conference on Wireless Technologies*, 2007, pp. 241–244.

[8] S. M. Asif, A. Iftikhar, J. W. Hansen, M. S. Khan, D. L. Ewert, and B. D. Braaten, "A novel rf-powered wireless pacing via a rectenna-based pacemaker and a wearable transmit-antenna array," *IEEE Access*, vol. 7, pp. 1139–1148, 2019.

[9] J. T. Bernhard, K. Hietpas, E. George, D. Kuchima, and H. Reis, "An interdisciplinary effort to develop a wireless embedded sensor system to monitor and assess corrosion in the tendons of prestressed concrete girders," in *2003 IEEE Topical Conference on Wireless Communication Technology*, 2003, pp. 241–243.

[10] X. Zhao, H. Gao, G. Zhang, B. Ayhan, F. Yan, C. Kwan, and J. L. Rose, "Active health monitoring of an aircraft wing with embedded piezoelectric sensor/actuator network: I. defect detection, localization and growth monitoring," *Smart Materials and Structures*, vol. 16, no. 4, pp. 1208–1217, jun 2007. [Online]. Available: https://doi.org/10.1088\%2F0964-1726\%2F16\%2F4\%2F032

[11] C. A. Balanis, *Antenna theory: analysis and design*. Wiley-Interscience, 2005.

[12] "Powercast company." [Online]. Available: https://www.powercastco.com/grips/

[13] M. Nie, X. Yang, G. Tan, and B. Han, "A compact 2.45-ghz broadband rectenna using grounded coplanar waveguide," *IEEE Antennas and Wireless Propagation Letters*, vol. 14, pp. 986–989, 2015.

[14] H. J. Visser and R. J. M. Vullers, "Wireless sensors remotely powered by rf energy," in *2012 6th European Conference on Antennas and Propagation (EUCAP)*, 2012, pp. 1–4.

[15] Y. Taryana, Y. Sulaeman, A. Setiawan, T. Praludi, and E. Hijriani, "Rectifying antenna design for wireless power transfer in the frequency of 2.45 ghz," in *2018 International Conference on Radar, Antenna, Microwave, Electronics, and Telecommunications (ICRAMET)*, 2018, pp. 55–58.

[16] G. Andia Vera, A. Georgiadis, A. Collado, and S. Via, "Design of a 2.45 ghz rectenna for electromagnetic (em) energy scavenging," in *2010 IEEE Radio and Wireless Symposium (RWS)*, 2010, pp. 61–64.

[17] A. Hirono, N. Sakai, and K. Itoh, “High efficient 2.4ghz band high power rectenna with the direct matching topology,” in *2019 IEEE Asia-Pacific Microwave Conference (APMC)*, 2019, pp. 1268–1270.

[18] C. Lin, C. Chiu, and J. Gong, “A wearable rectenna to harvest low-power rf energy for wireless health-care applications,” in *2018 11th International Congress on Image and Signal Processing, BioMedical Engineering and Informatics (CISP-BMEI)*, 2018, pp. 1–5.

[19] S. A. Maas, *Nonlinear microwave and RF circuits; 2nd ed.* Boston: Artech House, 2003. [Online]. Available: https://bib-pubdb1.desy.de/record/387459

[20] H. J. Visser, *Approximate Antenna Analysis for CAD*. Chichester, U.K: Wiley, 2009.

[21] M. M. Mansour and H. Kanaya, “Compact and broadband rf rectifier with 1.5 octave bandwidth based on a simple pair of l-section matching network,” *IEEE Microwave and Wireless Components Letters*, vol. 28, no. 4, pp. 335–337, 2018.

[22] *LQW03AW3N6C00*, Skyworks Solutions. [Online]. Available: https://www.murata.com/en-us/products/productdetail?partno=LQW03AW3N6C00%23

[23] *SMS7630 SERIES*, Skyworks Solutions, 2021. [Online]. Available: https://www.skyworksinc.com/-/media/SkyWorks/Documents/Products/201-300/Surface_Mount_Schottky_Diodes_200041AG.pdf

[24] *RT/duroid® 6006/6010LM*, Rogers Corporation. [Online]. Available: https://rogerscorp.com/-/media/project/rogerscorp/documents/advanced-connectivity-solutions/english/data-sheets/rt-duroid-6006-6010lm-laminate-data-sheet.pdf

[25] *Ultra Low Power Harvester Power Management IC with Boost Charger*, Texas Instruments, 2019. [Online]. Available: https://www.ti.com/store/ti/en/p/product/?p=BQ25570RGRR

[26] *MSP430FR596x, MSP430FR594x Mixed-Signal Microcontrollers*, Texas Instruments, 2019. [Online]. Available: https://www.ti.com/lit/ds/symlink/msp430fr5969.pdf?ts=1622520995734

[27] *TMP116 High-Accuracy, Low-Power, Digital Temperature Sensor With SMBus- and I2C-Compatible Interface*, Texas Instruments, May 2017. [Online]. Available: https://www.ti.com/lit/ds/symlink/tmp116.pdf?ts=1622565910533

[28] “Equipment authorization – rf device.” [Online]. Available: https://www.fcc.gov/oet/ea/rfdevice

[29] *Thin-Film RF/Microwave Capacitor Technology*, AVX Corporation. [Online]. Available: https://datasheets.avx.com/Accu-P.pdf

[30] *Chip Inductors – 0402CS (1005)*, Coilcraft. [Online]. Available: https://www.coilcraft.com/getmedia/f6cf468d-46eb-4342-9245-4b8b34f8d1bb/0402cs.pdf

[31] T. Paing, E. Falkenstein, R. Zane, and Z. Popovic, “Custom ic for ultra-low power rf energy harvesting,” in *2009 Twenty-Fourth Annual IEEE Applied Power Electronics Conference and Exposition*, 2009, pp. 1239–1245.

[32] D. Mishra, S. De, S. Jana, S. Basagni, K. Chowdhury, and W. Heinzelman, “Smart rf energy harvesting communications: challenges and opportunities,” *IEEE Communications Magazine*, vol. 53, no. 4, pp. 70–78, 2015.

[33] A. Boaventura, A. Collado, N. B. Carvalho, and A. Georgiadis, “Optimum behavior: Wireless power transmission system design through behavioral models and efficient synthesis techniques,” *IEEE Microwave Magazine*, vol. 14, no. 2, pp. 26–35, 2013.

A Conference Slides

Santa Clara University

Powering IoT Sensors with RF Energy Harvesting

Members: Austin Rothschild, Kristi Nguyen

Advisor: Dr. Kurt Schab

Santa Clara University

A. Rothschild, K. Nguyen | RFEH for IOT | May 13, 2021 | 1 / 23

Santa Clara University

Outline

A. Rothschild, K. Nguyen | RFEH for IOT | May 13, 2021 | 2 / 23

Santa Clara University

Background

- Number of connected IoT devices by 2030 expected to reach 125 billion [1]

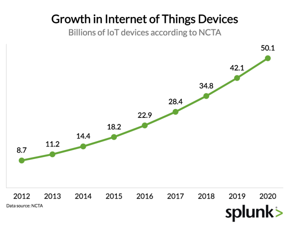

Current rise in IoT devices.

A. Rothschild, K. Nguyen | RFEH for IOT | May 13, 2021 | 3 / 23

Santa Clara University

Background

- Number of connected IoT devices by 2030 expected to reach 125 billion [1]
- Powering these devices w/ wired power grid infeasible due to *cabling costs* and *finite battery life*

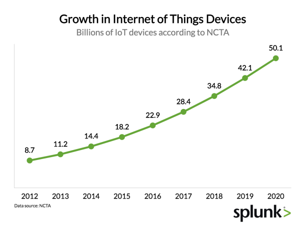

Current rise in IoT devices.

A. Rothschild, K. Nguyen | RFEH for IOT | May 13, 2021 | 3 / 23

Background

- Number of connected IoT devices by 2030 expected to reach 125 billion [1]
- Powering these devices w/ wired power grid infeasible due to *cabling costs* and *finite battery life*
  - An alternative power source is harvested *RF energy (RFEH)*

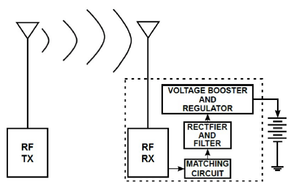

Idea *- Some transmitter (TX) delivers power which a receiver (RX) converts into a usable direct-current power source.*

Background

- Number of connected IoT devices by 2030 expected to reach 125 billion [1]
- Powering these devices w/ wired power grid infeasible due to *cabling costs* and *finite battery life*
  - An alternative power source is harvested *RF energy (RFEH)*
- System requirements of IoT devices which benefit from RFEH:
  1. Frequent battery replacement [2]
  2. Little maintenance [3]
  3. Device is difficult to access [4]

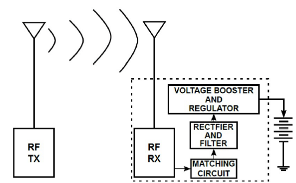

Idea *- Some transmitter (TX) delivers power which a receiver (RX) converts into a usable direct-current power source.*

Background

- Number of connected IoT devices by 2030 expected to reach 125 billion [1]
- Powering these devices w/ wired power grid infeasible due to *cabling costs* and *finite battery life*
  - An alternative power source is harvested *RF energy (RFEH)*
- System requirements of IoT devices which benefit from RFEH:
  1. Frequent battery replacement [2]
  2. Little maintenance [3]
  3. Device is difficult to access [4]

Project Goal

Design & validate an integrated RFEH system capable of efficiently powering a selected sensor load with a dedicated RF energy source.

Outline

Objectives

1. Design rectenna (rectifier + antenna) for RF-to-DC conversion
2. Manufacture and characterize custom PCB realization of design
3. Interface PCB with power management IC
4. Validate design by wirelessly powering temperature sensor

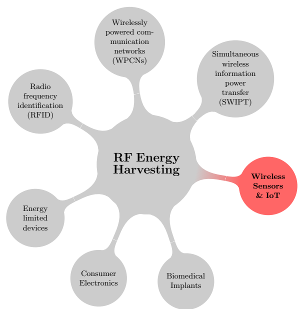

Outline

Project Schedule

Fall	
Weeks 1-4	Literature review
Weeks 5-6	Choose antenna, rectifier circuit, diode, load
Weeks 7-10	Simulate rectifier and antenna
Winter	
Weeks 1-3	Finalize rectifier and antenna simulations
Weeks 5-6	Power management unit integration & load
Weeks 7-10	Layout & fabrication
Spring	
Weeks 1-3	Tune antenna, rectifier, & characterize board performance
Weeks 4-5	Conducted/OTA Measurements, PMU/sensor integration
Weeks 6-7	Compile findings & final report

Functional Block Diagram

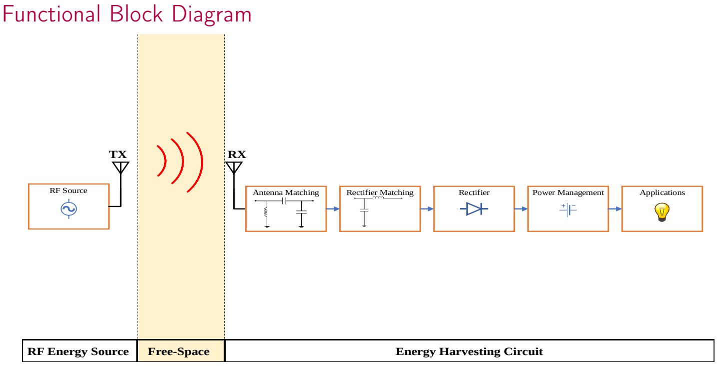

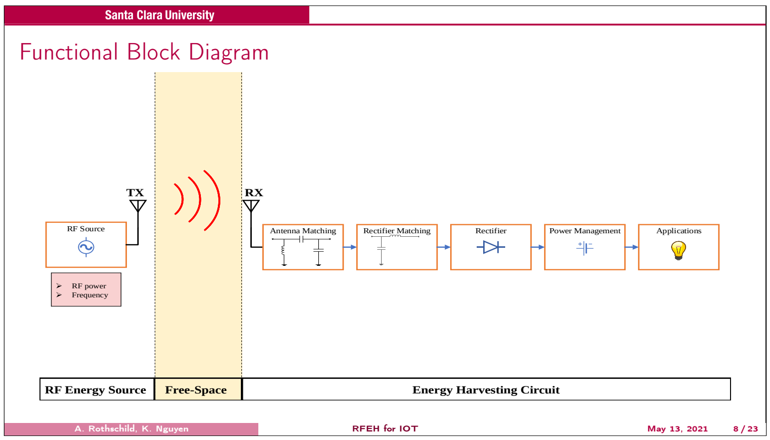
Santa Clara University
Functional Block Diagram
TX
RX
RF Source
RF power
Frequency
Antenna Matching
Rectifier Matching
Rectifier
Power Management
Applications
RF Energy Source
Free-Space
Energy Harvesting Circuit
A. Rothschild, K. Nguyen
RFEH for IOT
May 13, 2021
8 / 23

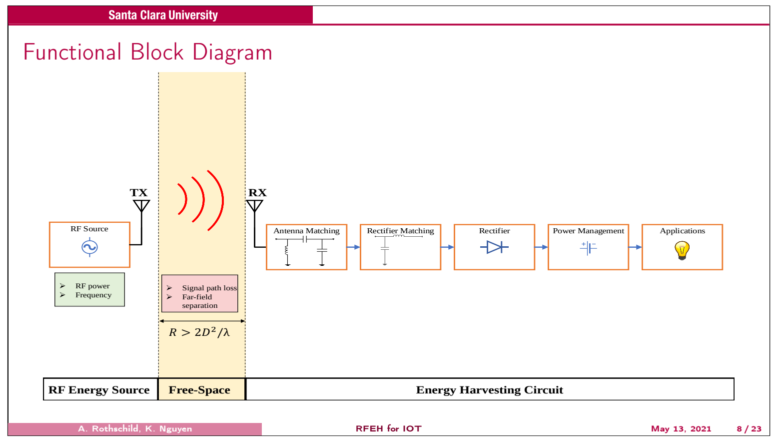
Santa Clara University
Functional Block Diagram
TX
RX
RF Source
RF power
Frequency
Signal path loss
Far-field separation
$R > 2D^2/\lambda$
Antenna Matching
Rectifier Matching
Rectifier
Power Management
Applications
RF Energy Source
Free-Space
Energy Harvesting Circuit
A. Rothschild, K. Nguyen
RFEH for IOT
May 13, 2021
8 / 23

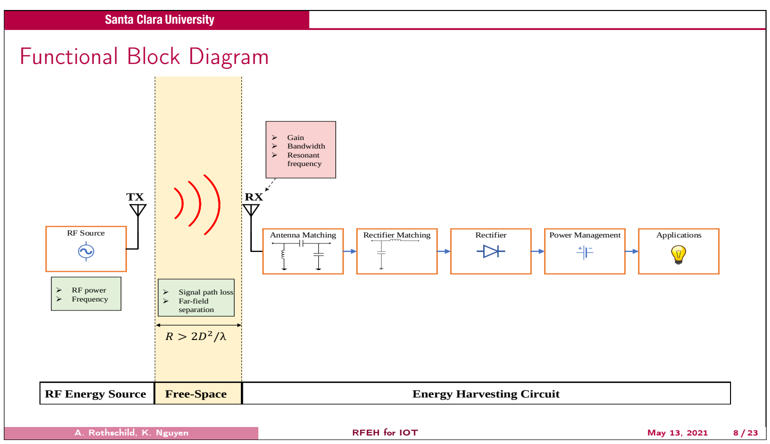
Santa Clara University
Functional Block Diagram
Gain
Bandwidth
Resonant frequency
TX
RX
RF Source
RF power
Frequency
Signal path loss
Far-field separation
$R > 2D^2/\lambda$
Antenna Matching
Rectifier Matching
Rectifier
Power Management
Applications
RF Energy Source
Free-Space
Energy Harvesting Circuit
A. Rothschild, K. Nguyen
RFEH for IOT
May 13, 2021
8 / 23

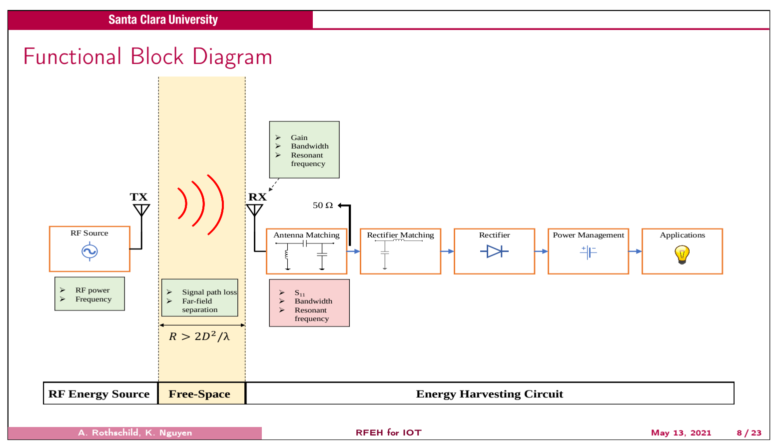
Santa Clara University
Functional Block Diagram
Gain
Bandwidth
Resonant frequency
TX
RX
50 Ω
RF Source
RF power
Frequency
Signal path loss
Far-field separation
$R > 2D^2/\lambda$
Antenna Matching
Rectifier Matching
Rectifier
Power Management
Applications
S_{11}
Bandwidth
Resonant frequency
RF Energy Source
Free-Space
Energy Harvesting Circuit
A. Rothschild, K. Nguyen
RFEH for IOT
May 13, 2021
8 / 23

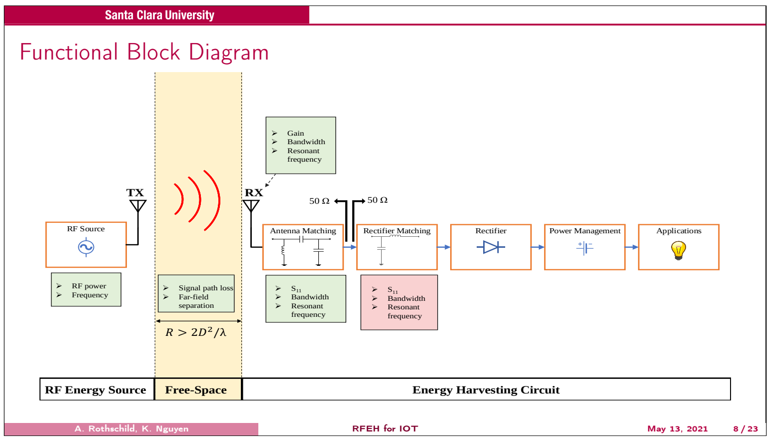
Santa Clara University
Functional Block Diagram
Gain
Bandwidth
Resonant frequency
TX
RX
50 Ω
50 Ω
RF Source
Antenna Matching
Rectifier Matching
Rectifier
Power Management
Applications
RF power
Frequency
Signal path loss
Far-field separation
$R > 2D^2/\lambda$
S_{11}
Bandwidth
Resonant frequency
S_{11}
Bandwidth
Resonant frequency
RF Energy Source
Free-Space
Energy Harvesting Circuit
A. Rothschild, K. Nguyen
RFEH for IOT
May 13, 2021
8 / 23

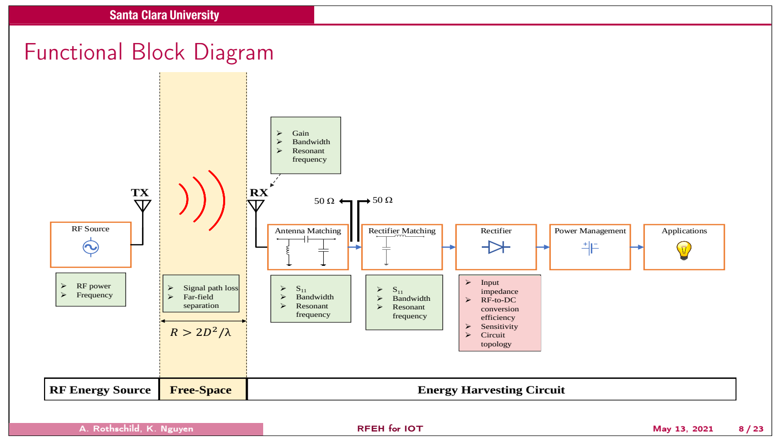
Santa Clara University
Functional Block Diagram
Gain
Bandwidth
Resonant frequency
TX
RX
50 Ω
50 Ω
RF Source
Antenna Matching
Rectifier Matching
Rectifier
Power Management
Applications
RF power
Frequency
Signal path loss
Far-field separation
$R > 2D^2/\lambda$
S_{11}
Bandwidth
Resonant frequency
S_{11}
Bandwidth
Resonant frequency
Input impedance
RF-to-DC conversion efficiency
Sensitivity
Circuit topology
RF Energy Source
Free-Space
Energy Harvesting Circuit
A. Rothschild, K. Nguyen
RFEH for IOT
May 13, 2021
8 / 23

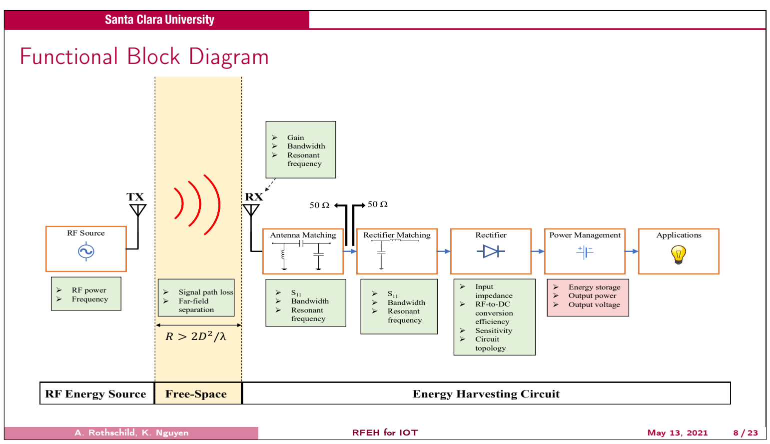
Santa Clara University
Functional Block Diagram
Gain
Bandwidth
Resonant frequency
TX
RX
50 Ω
50 Ω
RF Source
Antenna Matching
Rectifier Matching
Rectifier
Power Management
Applications
RF power
Frequency
Signal path loss
Far-field separation
$R > 2D^2/\lambda$
S_{11}
Bandwidth
Resonant frequency
S_{11}
Bandwidth
Resonant frequency
Input impedance
RF-to-DC conversion efficiency
Sensitivity
Circuit topology
Energy storage
Output power
Output voltage
RF Energy Source
Free-Space
Energy Harvesting Circuit
A. Rothschild, K. Nguyen
RFEH for IOT
May 13, 2021
8 / 23

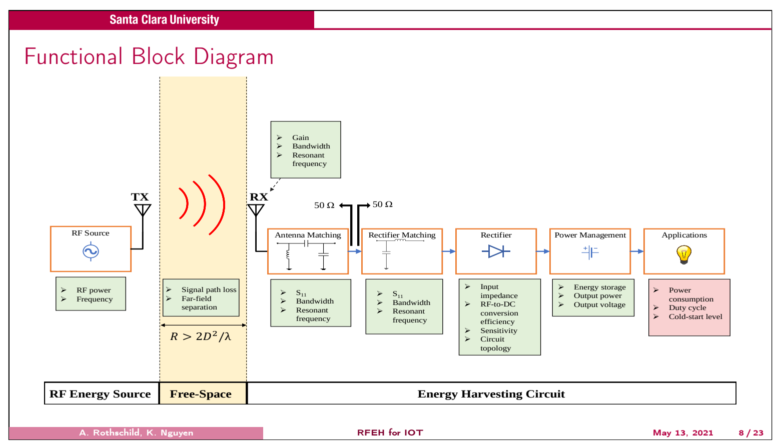
Santa Clara University
Functional Block Diagram
Gain
Bandwidth
Resonant frequency
TX
RX
50 Ω
50 Ω
RF Source
Antenna Matching
Rectifier Matching
Rectifier
Power Management
Applications
RF power
Frequency
Signal path loss
Far-field separation
$R > 2D^2/\lambda$
S_{11}
Bandwidth
Resonant frequency
S_{11}
Bandwidth
Resonant frequency
Input impedance
RF-to-DC conversion efficiency
Sensitivity
Circuit topology
Energy storage
Output power
Output voltage
Power consumption
Duty cycle
Cold-start level
RF Energy Source
Free-Space
Energy Harvesting Circuit
A. Rothschild, K. Nguyen
RFEH for IOT
May 13, 2021
8 / 23

Outline

Outcomes: PCB Rectenna

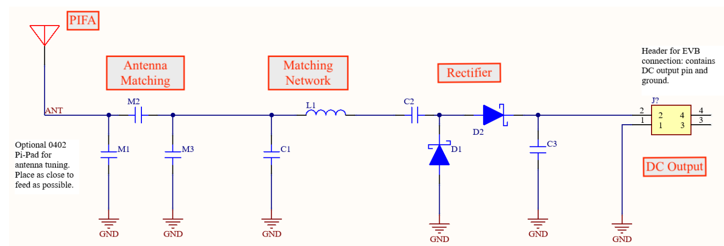

Custom rectenna schematic; designed in Altium.

Outcomes: PCB Rectenna

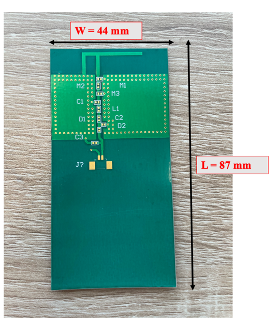

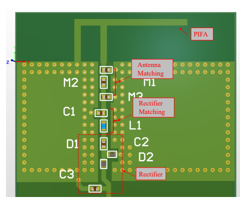

Substrate	Permittivity ϵ_r	Dielectric Height h	Trace Width w
Rodgers 6006	6.15	0.635 mm	0.935 mm

Outcomes: *Rectifier*

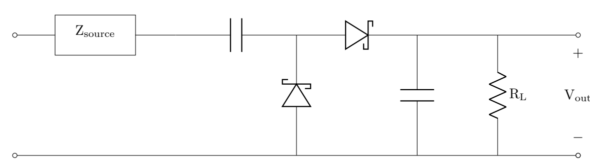

Voltage doubler schematic.

Outcomes: *Rectifier*

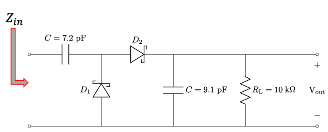

Schematic of circuit used for verify input impedance. Diodes are SMS7630-040LF, Capacitors are from Murata GCM15 series, Resistor is standard through-hole.

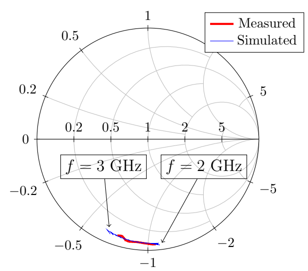

Simulated and measured input impedance $Z_{\rm in}$ at $P_{\rm in} = -10$ dBm, $R_{\rm L} = 10$ kΩ.

Outcomes: *Rectifier*

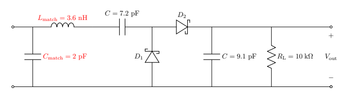

Rectifier circuit w/ matching component values obtained through ADS optimization and physical fine-tuning.

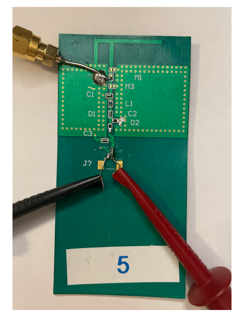

Rectifier match tuning setup for fixed input power $P_{\rm in} = -10$ dBm, $R_{\rm L} = 10$ kΩ.

Outcomes: *Rectifier*

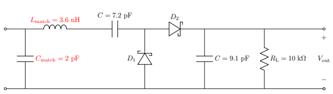

Rectifier circuit w/ matching component values obtained through ADS optimization and physical fine-tuning.

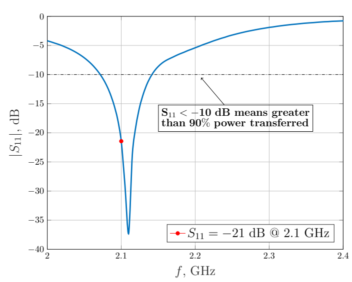

Matched rectifier S_{11} response for fixed input power $P_{\rm in} = -10$ dBm, $R_{\rm L} = 10$ kΩ.

Outcomes: *Rectifier*

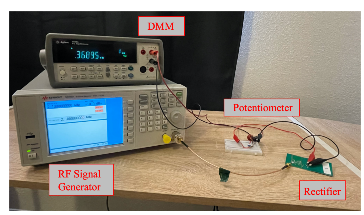

Rectifier characterization test setup.

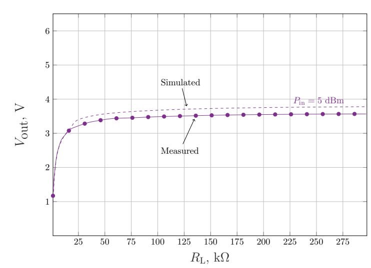

Outcomes: *Rectifier*

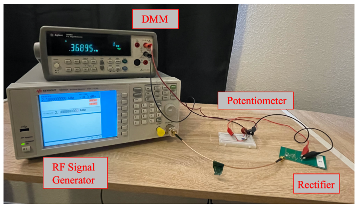

Rectifier characterization test setup.

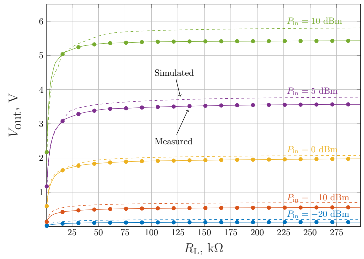

Outcomes: *Rectifier*

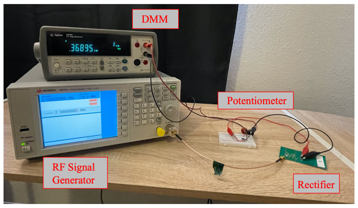

Rectifier characterization test setup.

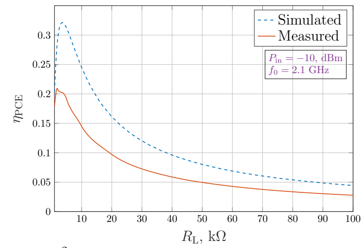

$$\eta_{PCE} = \frac{P_{DC}}{P_{in}} = \frac{V_{out}^2}{R_L \cdot P_{in}} \quad (1)$$

Outcomes: *Antenna*

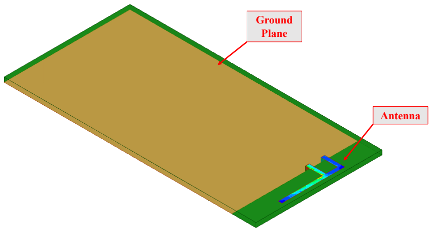

*Planar Inverted-F Antenna **(PIFA)** HFSS layout.*

Outcomes: *Antenna*

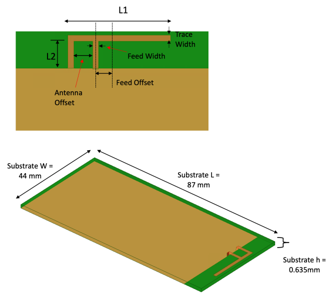

IFA w/ design dimensions.

L1 mm	L2 mm	Ant. Offset mm	Feed Offset mm	Feed Width mm	Trace Width mm
22.5	8.47	3.9	4.5	1.2	1.3

Outcomes: *Antenna*

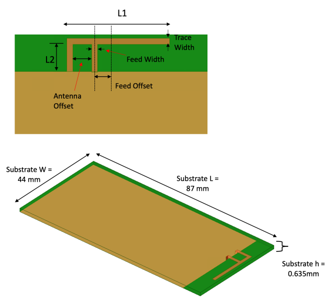

IFA w/ design dimensions.

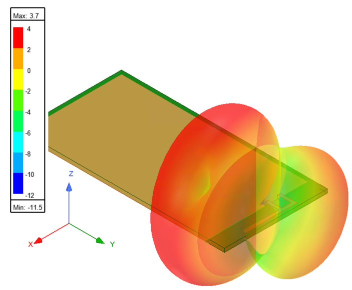

Simulated IFA gain pattern.

Outcomes: *Antenna*

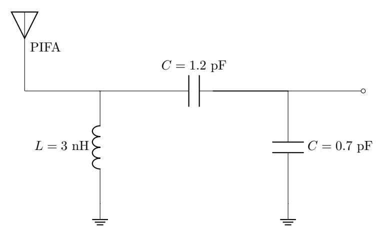

Lumped component values used to match antenna.

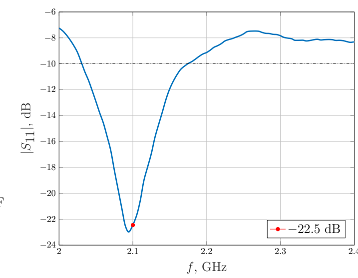

Matched antenna log-magnitude plot. $P_{in} = -10$ *dBm,* $R_L = 10$ kΩ.

Over-the-Air (OTA) Measurements

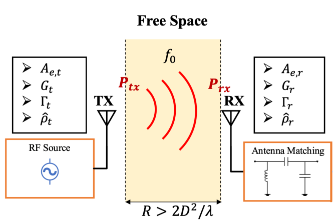

Device	Effective Aperture A_e	Gain G	Reflection Coefficient Γ	Polarization $\hat{\rho}$	Max Linear Dimension D
TX	513.6 cm^2	15 dBi	<-15 dB	Linear: vertical	20.6 cm
RX	38.1 cm^2	3.7 dBi	<-15 dB	Linear: horizontal/vertical	2.5 cm

Over-the-Air (OTA) Measurements

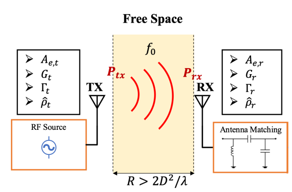

OTA Link Budget Block Diagram.

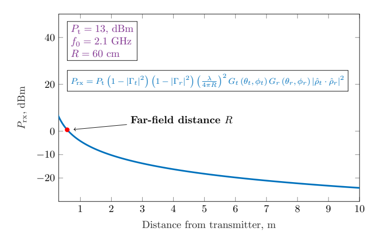

Received power vs. distance link-budget.

Santa Clara University

Over-the-Air (OTA) Measurements

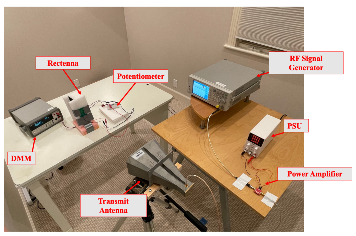

OTA Test Setup.

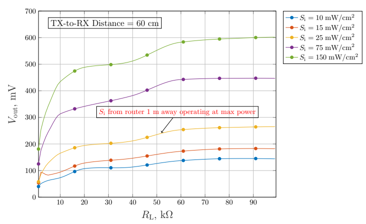

DC Output vs. different input power densities S_i. Higher voltage levels are unable to be achieved here due to TX amplifier saturation.

Santa Clara University

Application: Wirelessly Powered Temperature Sensor

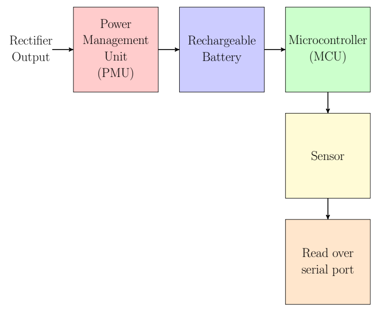

	PMU	MCU	Sensor
Min. Cold Start (V)	0.6	–	–
Min. Operation (V)	0.1	1.8	1.9

Specifications for sensor load.

Santa Clara University

OTA Sensor Test

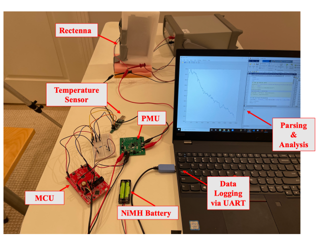

Rectenna with sensor load.

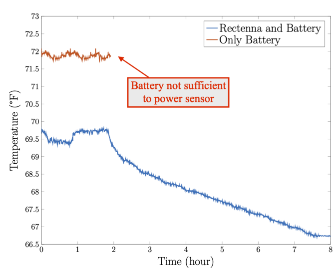

OTA test with sensor load vs. only sensor load over 8 hours.

Santa Clara University

Outline

Project Adaptation

- Initially designed system for $f_0 = 2.45$ GHz

Project Adaptation

- Initially designed system for $f_0 = 2.45$ GHz
- Antenna matched simulated behavior

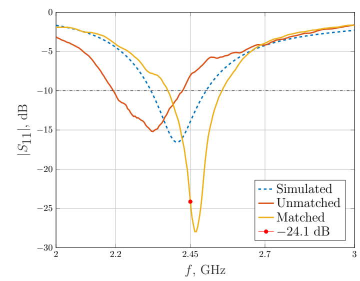

Project Adaptation

- Initially designed system for $f_0 = 2.45$ GHz
- Antenna matched simulated behavior
- Rectifier was not able to be matched at 2.45 GHz initially
  - Issue due to SMD capacitors/inductors used

Project Adaptation

- Initially designed system for $f_0 = 2.45$ GHz
- Antenna matched simulated behavior
- Rectifier was not able to be matched at 2.45 GHz initially
  - Issue due to SMD capacitors/inductors used
- Switching to higher frequency rated components, rectifier able to be matched

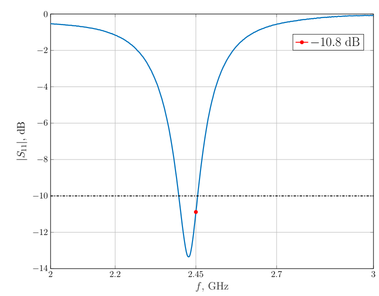

Project Adaptation

- Initially designed system for $f_0 = 2.45$ GHz
- Antenna matched simulated behavior
- Rectifier was not able to be matched at 2.45 GHz initially
  - Issue due to SMD capacitors/inductors used
- Switching to higher frequency rated components, rectifier able to be matched
- Due to timing, system tests/characterization were performed with an optimized 2.1 GHz rectenna

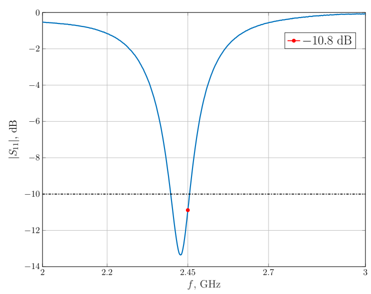

Performance Assessment

Objectives	Status	Source of Error
Design rectifier and antenna for RF-to-DC conversion	✓	–
Layout PCB, fabricate PCB, and tune antenna	✓	–
Implement matching networks	Antenna is well-matched; rectifier could not initially be matched for 2.45 GHz	Needed components with higher SRF
Measure and validate	✓	–
Integrate rectenna with sensor load	Yes, but cannot reliably operate in cold-start mode	PMU input impedance differed from expected ($R_L = 10$ kΩ); Varies depending on PMU state

Reliability and Sustainability

Pros	Cons	Performance Enhancements
• Easy to manufacture; small size • *Sustainable* alternative to other energy sources	• Parasitics & process variation of PCB/components • Equivalent DC load impedance • Storage element current leakage	• Custom PMU ASIC's [5] • TX/RX beamforming [6] • Custom transmit signal properties [7]

Outline

Summary and Conclusions

Project Objective

Design & validate RFEH system capable of sufficiently powering an IoT sensor.

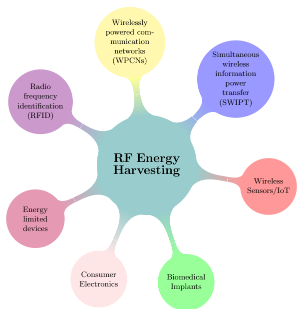

Summary and Conclusions

Project Objective

Design & validate RFEH system capable of sufficiently powering an IoT sensor.

- **Outcomes**
  - Robust antenna & rectifier simulations
  - Custom PCB realization of design
  - Validation of design via measurements & application to a practical use-case

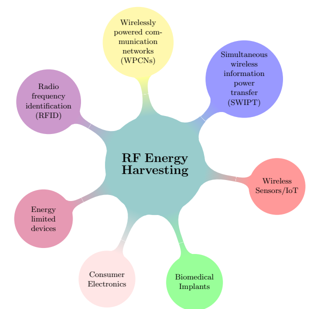

Summary and Conclusions

Project Objective

Design & validate RFEH system capable of sufficiently powering an IoT sensor.

- **Outcomes**
  - Robust antenna & rectifier simulations
  - Custom PCB realization of design
  - Validation of design via measurements & application to a practical use-case
- **Future Work**
  - EM co-simulation of PCB + diode models
  - Integration of PMU + sensor onto remaining PCB area
  - OTA characterization in controlled environment (anechoic chamber)
  - Exploration of input signal optimization

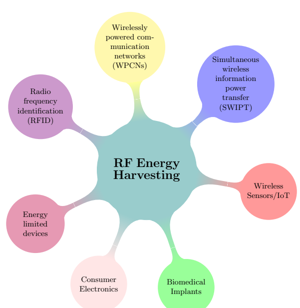

References

[1] T. Jury, "How many iot devices are there in 2020?" [Online]. Available: https://techjury.net/blog/how-many-iot-devices-are-there/

[2] M. Z. Chaari and S. Al-maadeed, "Wireless power transmission for the internet of things (iot)," in *2020 IEEE International Conference on Informatics, IoT, and Enabling Technologies (ICIoT)*, 2020, pp. 549–554.

[3] S. M. Asif, A. Iftikhar, J. W. Hansen, M. S. Khan, D. L. Ewert, and B. D. Braaten, "A novel rf-powered wireless pacing via a rectenna-based pacemaker and a wearable transmit-antenna array," *IEEE Access*, vol. 7, pp. 1139–1148, 2019.

[4] X. Zhao, H. Gao, G. Zhang, B. Ayhan, F. Yan, C. Kwan, and J. L. Rose, "Active health monitoring of an aircraft wing with embedded piezoelectric sensor/actuator network: I. defect detection, localization and growth monitoring," *Smart Materials and Structures*, vol. 16, no. 4, pp. 1208–1217, jun 2007. [Online]. Available: https://doi.org/10.1088%2F0964-1726%2F16%2F4%2F032

[5] T. Paing, E. Falkenstein, R. Zane, and Z. Popovic, "Custom ic for ultra-low power rf energy harvesting," in *2009 Twenty-Fourth Annual IEEE Applied Power Electronics Conference and Exposition*, 2009, pp. 1239–1245.

[6] D. Mishra, S. De, S. Jana, S. Basagni, K. Chowdhury, and W. Heinzelman, "Smart rf energy harvesting communications: challenges and opportunities," *IEEE Communications Magazine*, vol. 53, no. 4, pp. 70–78, 2015.

[7] A. Boaventura, A. Collado, N. B. Carvalho, and A. Georgiadis, "Optimum behavior: Wireless power transmission system design through behavioral models and efficient synthesis techniques," *IEEE Microwave Magazine*, vol. 14, no. 2, pp. 26–35, 2013.

Outline

Extra: Rectifier Efficiency Contours

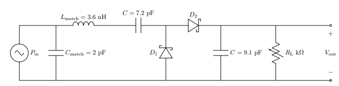

Matched rectifier circuit w/ variable input power and output load control.

- Efficiency is maximized for a particular combination of load impedance & input power.
- The *goal* is to keep the rectifier operating in this region while active.

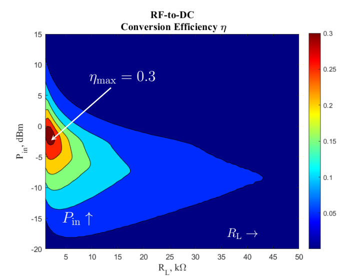

Simulated contours of efficiency as a function of load resistance and input power.

Extra: Matched Antenna Smith Chart

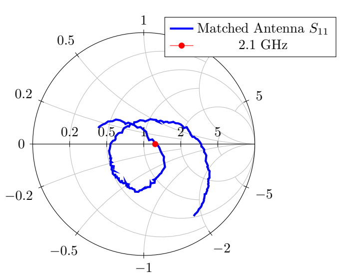

Matched antenna smith chart. $f_0 = 2.1$ *GHz,* $P_{\mathrm{in}} = -10$ *dBm,* $R_{\mathrm{L}} = 10$ kΩ.

Extra: Sensor Load Schematics

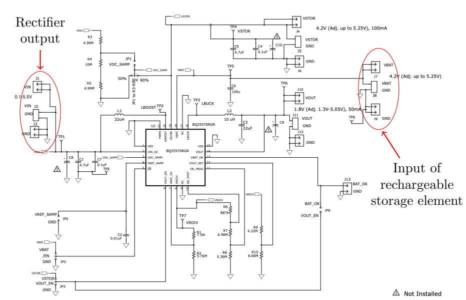

BQ25570 PMU Schematic.

Extra: Sensor Load Schematics

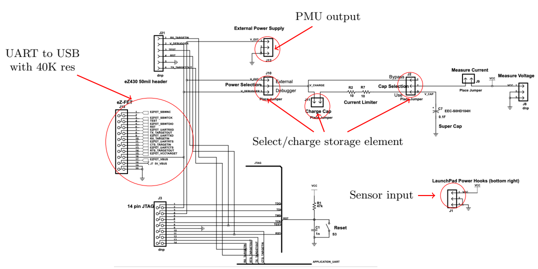

MSP430 Microcontroller Schematic.

Extra: Sensor Load Schematics

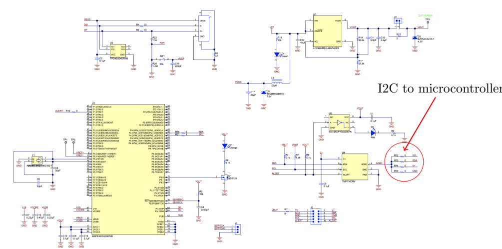

TMP116 Sensor Schematic.

Extra: OTA Sensor Test Conditions

P_{tx}	13dBm
P_{rx}	-5dBm
Distance from transmitter	10.5cm
Sampling frequency	1 measurement/5 seconds

OTA sensor evaluation test conditions.

B Equipment & Software

This section details design tools, software, and measuring equipment.

Tool	Category	Purpose
Vector Network Analyzer	Equipment	Measure rectifier impedance.
Spectrum Analyzer	Equipment	Measure rectenna received power.
Digital Multi-meter	Equipment	Measure DC voltage output.
RF Signal Generator	Equipment	Generate continuous wave RF signals at various power levels.
Advanced Design Software (ADS)	Software	Design & simulate rectifier.
High Frequency Structure Simulator (HFSS)	Software	Design & simulate antenna.
Energia	Software	Integrated Design Environment (IDE) for MSP430 microcontroller.
MATLAB	Software	Log sensor data.

Table 8: Simulation software and measurement equipment needed for project design and validation.

C Temperature Sensor Pin-outs & Code

C.1 Schematics and Wiring Table

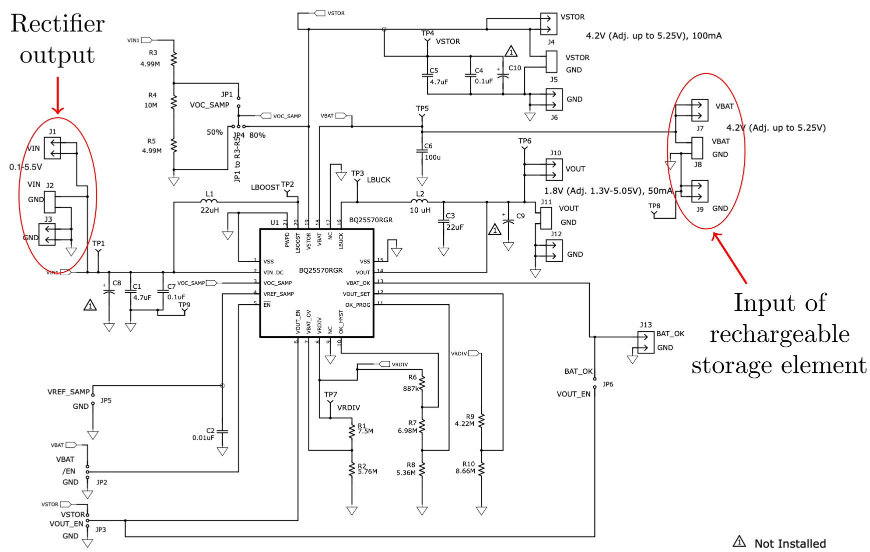

Figure 30: Annotated schematic of PMU, TIBQ25570 Evaluation Module.

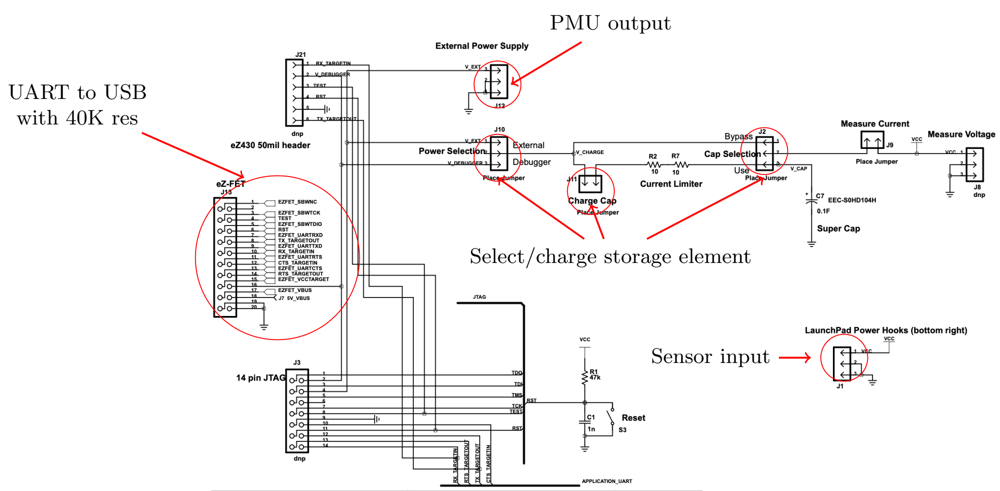

Figure 31: Annotated schematic of microcontroller, MSP430FR5969 Launchpad.

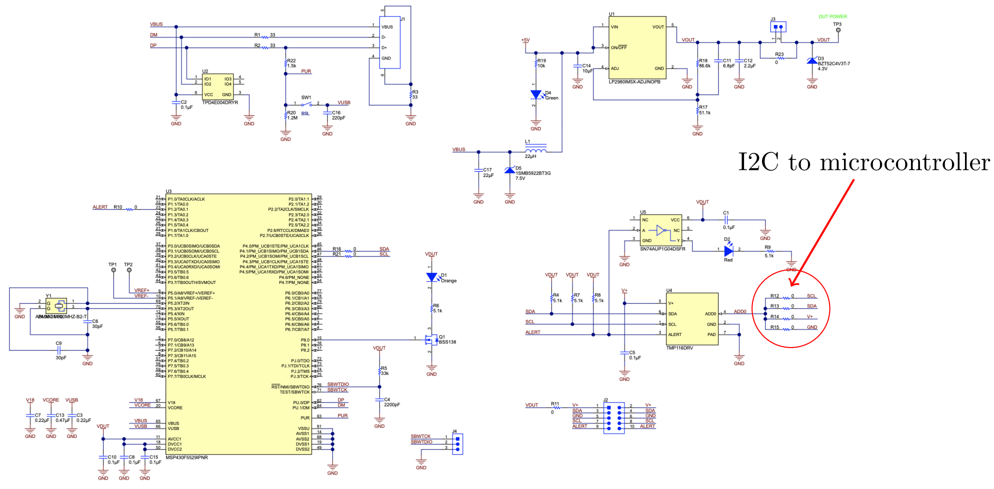

Figure 32: Annotated schematic of temperature sensor, TMP116 Evaluation Module.

Pin	Function	Notes
TIBQ25570 Evaluation Module: Interfacing with rectifier and battery		
J2	Connect to rectifier output	Input source terminal block
J8	Connect to storage element input	Rechargeable storage element terminal block
JP4	Configure to 80% ratio	Maximum powerpoint tracking feature
JP2	Connect to GND to enable IC.	Enable/disable IC. Should always be enabled
MSP430FR5969 Launchpad: Programming		
J13	Connect horizontal jumpers across RXD, TXD, 5V, GND, V+, RST, TST on J13	Program using USB to UART cable assembly
MSP430FR5969 Launchpad: Reading data		
J13 RXD	Connect to UART TXD	Read serial port with computer using USB to UART wires
J13 TXD	Connect to UART RXD	
J13 GND	Connect to UART GND	
J13 5V	Connect to UART V+	
MSP430FR5969 Launchpad: Connecting to battery		
J10	Connect jumper to ”external”	”Debugger” will charge via computer, ”external” will charge through external power
J2	Connect jumper to ”bypass”	”Use” will use the microcontroller’s supercapacitor, ”bypass” will use a different power source
J11	Remove jumper	Jumper across J11 will charge the supercapacitor
J12	Connect to external power supply	External power supply terminal block
J13 GND	Connect 30-40KΩ resistor in between J13 GND and UART GND	Prevent microcontroller/temperature sensor from being powered by the computer
TMP116 Evaluation Module: Interfacing with microcontroller		
R12	Connect to MSP SCL	I2C clock line
R13	Connect to MSP SDA	I2C data line
R14	Connect to MSP V+	
R15	Connect to MSP GND	

Table 9: Sensor load pin-outs.

C.2 Code

C.2.1 Temperature Sensor Reading

```
/*
 *  TMP116_Example.ino
 *  Developed by Megan Anderson, THS Applications Engineering Intern
 *  May 2018
 *
 *  Adapted by Kristi Nguyen and Austin Rothschild for Powering IoT Sensors with
 *  RF Energy Harvesting
 *
 *  Purpose: Interface MSP430 with the TMP116 temperature sensor to measure the
 *  temperature and send over serial port. Device communicates information based
 *  on I2C protocol.
 *
 *  This was originally written for Arduino, but can be used with Energia (IDE for MSP
    controllers)
 *  Original link: https://training.ti.com/how-interface-tmp116-tmp117-temperature-
    sensors-arduino
 */

 #include <Wire.h>
 #include <LiquidCrystal.h>

 volatile int alarm;

 // Device address
 const int TMP116_Address = 0x48;

 // Hexadecimal addresses for various TMP116 registers
 const int Temp_Reg = 0x00;            // Temperature register
 const int Config_Reg = 0x01;          // Configuration register
 const int High_Lim_Reg = 0x02;        // High limit register
 const int Low_Lim_Reg = 0x03;         // Low limit register
 const int EEPROM_Unlock_Reg = 0x04;   // EEPROM unlock register
 const int Device_ID_Reg = 0x0F;       // Device ID register

 // Set temperature threshold
 const uint8_t highlimH = B00001101;   // High byte of high lim
 const uint8_t highlimL = B10000000;   // Low byte of high lim  - High 27 C
 const uint8_t lowlimH = B00001100;    // High byte of low lim
 const uint8_t lowlimL = B00000000;    // Low byte of low lim   - Low 24 C

// delay time
const double delaytime = 5000; // 5 seconds;

 // Declare pin assignments for LCD in order: RS, E, D4, D5, D6, D7
 LiquidCrystal lcd(7,8,9,10,11,12);

/************************* Initialization Setup Function *************************/
 void setup(){

  // Initiate wire library and serial communication
  Wire.begin();
  Serial.begin(9600);

  // Initialize LCD
  lcd.begin(16,2);
  lcd.home();
  lcd.print("Temp(C): ");

  // Write to register
  I2Cwrite(TMP116_Address, High_Lim_Reg, highlimH, highlimL);
  I2Cwrite(TMP116_Address, Low_Lim_Reg, lowlimH, lowlimL);
  I2Cwrite(TMP116_Address, Config_Reg,0x02, 0x20);

```

```
  // Sets Pin 13 as output, Pin 2 as input (active low)
  pinMode(13, OUTPUT);
  pinMode(2, INPUT_PULLUP);

  // Sets up pin 2 to trigger "alert" ISR when pin changes H->L and L->H
  attachInterrupt(digitalPinToInterrupt(2), alert, CHANGE);

  alarm = digitalRead(2); // reads startup ALERT pin value
 }

/************************* Infinite Loop Function **********************************/
 void loop(){
  // Calls ReadSensor function to get temperature data
  double temp = ReadTempSensor();

  // Sets cursor at 9th column, 0th row
  lcd.setCursor(9,0);
  lcd.print(temp);
  Serial.print(temp); // Print to serial monitor, this code works w/o LCD
  Serial.print("\n");

  if (!alarm){ // If alarm is active low, trigger alert
    digitalWrite(13,HIGH);
    lcd.setCursor(9,1);
    lcd.print("ALERT");

    // Clear ALERT flag by I2C reading from config reg
    Wire.beginTransmission(TMP116_Address);
    Wire.write(Config_Reg);
    Wire.endTransmission();
    delay(10);
    Wire.requestFrom(TMP116_Address,2);
  }
  else{ // Turn alert off
    digitalWrite(13,LOW);
    lcd.setCursor(9,1);
    lcd.print("     ");
  }

  // Delay (500 = 0.5 second)
  delay(delaytime);
 }

/********************** Read Temperature Sensor Function *************************/
double ReadTempSensor(void){

  // Data array to store 2-bytes from I2C line
  uint8_t data[2];
  // Combination of 2-byte data into 16-bit data
  int16_t datac;

  // Points to device & begins transmission
  Wire.beginTransmission(TMP116_Address);
  // Points to temperature register to read/write data
  Wire.write(Temp_Reg);
  // Ends data transfer and transmits data from register
  Wire.endTransmission();

  // Delay to allow sufficient conversion time
  delay(10);

  // Requests 2-byte temperature data from device
  Wire.requestFrom(TMP116_Address,2);
```

```

  // Checks if data received matches the requested 2-bytes
  if(Wire.available() <= 2){
    // Stores each byte of data from temperature register
    data[0] = Wire.read();
    data[1] = Wire.read();

    // Combines data to make 16-bit binary number
    datac = ((data[0] << 8) | data[1]);

    // Convert to Farenheit (7.8125 mC resolution) and return
    return datac*0.0078125*9/5+32;

  }
}

/**************************** I2C Write Function ********************************/
double I2Cwrite(int dev, int reg, int H, int L){
  // Takes in 4 variables:
  // device address, register addres
  // high and low bytes of data to transmit
  Wire.beginTransmission(dev);
  Wire.write(reg);
  Wire.write(H);
  Wire.write(L);
  Wire.endTransmission();
  delay(10);
}

/******************************* ALERT ISR **************************************/

void alert(){

  alarm = digitalRead(2);

}
```

Listing 1: MSP430 and TMP 116 code.

C.2.2 Data Logging and Post-Processing

```

clear
close all
clc

%% Set up serial port

port = "/dev/cu.SLAB_USBtoUART";
%port = "/dev/cu.usbmodem141103";
baudrate=9600;
dayInSeconds = 8*60*60;
stoptime = dayInSeconds;

%% Set up Post-Processing
filename = ['sensor_',char(datetime('today')),'.csv'];
str = struct;
flag = 0;

%% Read data and stop after reaching certain time

i = 1;
```

```
tic
while 1

    try
        s = serialport(port,baudrate);
    catch
        % continue to rest of loop
    end

    try % this needs to be in separate 'try' because serialport yields error
        % if matlab has already opened serialport
        str.numdata(i,1) = str2num(readline(s));
        str.date(i,1) = datetime('now');
    catch
        % continue to rest of loop
    end

  timestamp = toc;

  if timestamp >= stoptime % tic toc is in seconds
      flag = 1;
      T = struct2table(str);
      writetable(T,filename);
      break;
  end

  i = i+1;

end

%% Make graph

if flag == 0 % if you stop code before stoptime
    T = struct2table(str);
    writetable(T,filename);
end

numdata = str.numdata;

xaxis = 0:1:length(numdata)-1;
xaxis = xaxis*5/60;

figure(101)
plot(xaxis,numdata)
ylabel('Temperature (degrees F)')
xlabel('Time (hour)')
title('Temperature over Time')
```

Listing 2: Log data over serial port and save to CSV file.